Vangl2/RhoA signaling regulates stem cell self-renewal programs and growth in Rhabdomyosarcoma

Madeline N Hayes, Karin Mccarthy, Alexander Jin, Mariana L Oliveira, Sowmya Iyer, Sara P Garcia, Sivasish Sindiri, Berkley Gryder, Zainab Motala, G Petur Petur Nielsen, et al.

Vangl2/RhoA signaling regulates stem cell self-renewal programs and growth in Rhabdomyosarcoma.

Madeline N. Hayes[1,2], Karin McCarthy[1,2], Alexander Jin[1,2], Mariana L. Oliveira[1,2,3], Sowmya Iyer[1,2], Sara P. Garcia[1,2], Sivasish Sindiri[4], Berkley Gryder[4], Zainab Motala[5], G. Petur Nielsen[6], Jean-Paul Borg[7], Matt van de Rijn[8], David Malkin[5], Javed Khan[4], Myron S. Ignatius[9], David M. Langenau[1,2,*]

[1]Molecular Pathology, Cancer Center, and Regenerative Medicine, Massachusetts General Hospital Research Institute, Boston, MA 02129, USA; [2]Harvard Stem Cell Institute, Cambridge, MA 02139, USA; [3]Instituto de Medicina Molecular, Faculdade de Medicina, Universidade de Lisboa, 1649-028, Lisbon, Portugal; [4]Oncogenomics Section, Center for Cancer Research, National Cancer Institute, NIH, 37 Convent Drive, Bethesda, MD 20892, USA; [5]Division of Hematology/Oncology, Hospital for Sick Children and Department of Pediatrics, University of Toronto, Toronto, Ontario M5G1X8, Canada; [6]Department of Pathology, Massachusetts General Hospital, Boston, MA 02129, USA; [7]Centre de Recherche en Cancérologie de Marseille, Aix Marseille Univ UM105, Inst Paoli Calmettes, UMR7258 CNRS, U1068 INSERM, «Cell Polarity, Cell signalling and Cancer - Equipe labellisée Ligue Contre le Cancer», Marseille, France; [8]Department of Pathology, Stanford University Medical Center, Stanford, CA 94305, USA; [9]Molecular Medicine and Greehey Children's Cancer Research Institute, UTHSCSA, San Antonio, TX, USA, 78229

*Corresponding Author and Lead Contact: dlangenau@mgh.harvard.edu

Summary

Tumor growth and relapse are driven by tumor propagating cells (TPCs). However, mechanisms regulating TPC fate choices, maintenance and self-renewal are not fully understood. Here, we show that Van Gogh-like 2 (Vangl2), a core regulator of the non-canonical Wnt/Planar Cell Polarity (Wnt/PCP) pathway, affects TPC self-renewal in rhabdomyosarcoma (RMS) – a pediatric cancer of muscle. VANGL2 is expressed in a majority of human RMS and within early mononuclear progenitor cells. VANGL2 depletion inhibited cell proliferation, reduced TPC numbers, and induced differentiation of human RMS *in vitro* and in mouse xenografts. Using a zebrafish model of embryonal rhabdomyosarcoma (ERMS), we identified that Vangl2 expression enriches for TPCs and promotes their self-renewal. Expression of constitutively active and dominant negative isoforms of RHOA revealed that it acts downstream of VANGL2 to regulate proliferation and maintenance of TPCs in human RMS. Our studies offer insights into pathways that control TPCs and identify new potential therapeutic targets.

Key words: Muscle, cancer, planar cell polarity, RhoA, zebrafish

Introduction

Continued tumor growth and relapse are driven by tumor propagating cells (TPCs) that share self-renewal properties with non-transformed stem cells (Kreso and Dick, 2014). For example, TPCs undergo self-renewal cell divisions to produce daughter cells with identical characteristics, ultimately expanding the pool of cells capable of driving tumor growth, elevating metastasis, and evading therapy (Kreso and Dick, 2014). TPCs can also divide asymmetrically to maintain the overall number of tumor-sustaining cells while also producing differentiated cells that have specialized functions necessary to support cancer progression and invasion (Ignatius et al., 2012; Kreso and Dick, 2014). Despite shared commonalities with normal stem cells, the molecular mechanisms regulating TPC fate specification, proliferation and self-renewal are largely unknown, especially in pediatric sarcomas (Dela Cruz, 2013; Friedman and Gillespie, 2011). In addition, identifying molecular markers of TPCs has been elusive in many cancer cell types, making specific characterization and therapeutic targeting difficult to achieve in the clinical setting. Yet, it is clear that TPCs drive tumor growth and are retained in a subset of patients to cause local relapse and metastasis (Dela Cruz, 2013; Kreso and Dick, 2014). Thus, there is strong impetus to identify molecularly defined TPCs, understand the mechanisms that regulate proliferation and self-renewal, and uncover genetic vulnerabilities that can be exploited to differentiate and/or kill these tumor-sustaining cells.

The Wnt/Planar Cell Polarity (Wnt/PCP) signaling pathway is essential during embryogenesis and for tissue homeostasis in adults (Seifert and Mlodzik, 2007). Wnt/PCP signaling acts independent of β-catenin and is regulated by pathway specific components such as Van Gogh (VANGL1 and VANGL2 in humans) that restrict Wnt/Frizzled activity to polarize epithelium and orient the motility of mesendodermal tissues (Peng and Axelrod, 2012; Seifert and Mlodzik, 2007). Vangl2 is a predicted four-pass transmembrane protein, yet lacks any known receptor or enzymatic activity (Murdoch, 2001). Rather protein-protein

interaction domains of Vangl2 modulate downstream signaling, including the activation of Rac1 and RhoA (Schlessinger et al., 2009; Seifert and Mlodzik, 2007). Despite well-known roles for the Wnt/PCP pathway during development, defined roles in cancer are just now beginning to emerge. For example, oncogenic roles for non-canonical Wnt proteins have been linked to elevated cell motility, increased metastasis, and reduced patient survival in breast, liver, colon, and lung cancer (Gujral et al., 2014; Puvirajesinghe et al., 2016; Yagyu et al., 2002). Yet, a specific role for Wnt/PCP components in regulating TPC fate or expanding overall pools of tumor-sustaining cell types has not been established.

Rhabdomyosarcoma (RMS), a pediatric cancer of muscle, has emerged as a powerful experimental platform to assess cancer stem cell biology and to identify novel paradigms for cancer growth that extend to a wide array of malignancies (Ignatius et al., 2012; Satheesha et al., 2015; Walter et al., 2011). RMS is comprised of two main molecular subtypes. Alveolar RMS (ARMS) display characteristic genomic translocations of the PAX3-FOXO1 or PAX7-FOXO1 loci accompanied by few additional genomic changes (Shern et al., 2014). In contrast, RAS pathway activation is the dominant oncogenic driver in 90% of human embryonal RMS (ERMS) (Chen et al., 2013; Langenau et al., 2007; Shern et al., 2014). Both RMS subtypes exhibit features of skeletal muscle arrested at early stages of embryonic development and display molecular characteristics consistent with a block in differentiation within the myogenic hierarchy. Importantly, TPCs have been identified in human and animal models of ERMS (Ignatius et al., 2012; Langenau et al., 2007; Satheesha et al., 2015; Walter et al., 2011). For example, we have used a fluorescent transgenic zebrafish model of *kRASG12D*-induced ERMS to define markers of intra-tumor heterogeneity and to isolate molecularly-defined TPCs (Ignatius et al., 2012; Langenau et al., 2007). Importantly, the same developmental hierarchies controlling muscle regeneration are recapitulated in ERMS, with TPCs sharing similar molecular pathway activation and gene expression markers with

activated muscle satellite stem cells. Building on these commonalities, we have identified Wnt/β-catenin, Notch, and myogenic transcription factor signaling pathways as modulators of TPC function in embryonal rhabdomyosarcoma, a role that is conserved from zebrafish to human (Chen et al., 2014; Ignatius et al., 2017; Tenente et al., 2017). This work highlights the power of the zebrafish model to characterize conserved stem cell pathways that drive TPC growth and maintenance that are shared in development, regeneration, and cancer.

Here, we show that VANGL2 is highly expressed in a large majority of primary human RMS and within the proliferating RMS progenitor-like cells. VANGL2 depletion led to decreased cell proliferation, reduced *in vitro* sphere colony formation, and differentiation of ERMS cells *in vitro.* Moreover, VANGL2 was required for continued xenograft growth and maintenance following engraftment of human RMS into mice. Using the *kRASG12D*-induced zebrafish ERMS model and fluorescent transgenic approaches to label RMS cells based on cellular differentiation status, we defined roles for Vangl2 in regulating TPC self-renewal and growth. Studies in human RMS showed that RHOA functions downstream of VANGL2 to regulate *in vitro* growth and sphere colony formation, a surrogate for self-renewal in ERMS. This mechanistic link between VANGL2, RHOA and TPC biology suggests mechanisms that drive RMS growth by specifically modulating a highly conserved stem cell self-renewal program.

Results

VANGL2 is highly expressed in human rhabdomyosarcoma

We previously identified a role for activated canonical Wnt/β-catenin signaling in driving differentiation of human RMS (Chen et al., 2014). Wnt/β-catenin signaling is normally suppressed in RMS and activation leads to TPC differentiation, reduced self-renewal, and suppressed tumor growth both *in vitro* and in animal models. Given that Wnt/β-catenin signaling also drives terminal differentiation in normal muscle development and can be antagonized by non-canonical Wnt pathways (Brack et al., 2008; Mccoy et al., 2011; Nemeth et al., 2007), we investigated the possibility that alternative Wnt signaling pathway components affect RMS tumor biology.

RNAseq data (GSE108022) from primary patient samples described in Shern et al. 2014 was analyzed. 151 genes from the GSEAsig database (KEGG_WNT_SIGNALING_PATHWAY) and others from the literature that represent Wnt signaling molecules or targets were selected and each was assessed for expression in human RMS subtypes. From this analysis, we identified significant upregulation of genes associated with the non-canonical Wnt/Planar Cell Polarity (Wnt/PCP) signaling pathway in both fusion-negative and fusion-positive RMS (Figure 1A). This included upregulation of Wnt ligands (*WNT5B, WNT7A/B)*, Frizzled receptors (*FZD2)* and regulatory proteins (*CELSR1/3, VANGL2* and *PTK7*) (Figure 1A, $p<0.01$). We were particularly interested in *VANGL*2, since Vangl proteins are essential regulators of Wnt/PCP signaling that have been well characterized in development and regeneration (von Maltzahn et al., 2012; Seifert and Mlodzik, 2007). Moreover, unlike Wnt ligands and Frizzled receptors, Vangl proteins display

minimal cross talk with the Wnt/β-catenin signaling pathway, making them useful targets to specifically interrogate Wnt/PCP signaling.

Analysis of RNA sequencing data revealed that *VANGL2* was upregulated in nearly all human RMS, regardless of subtype (n=61 of 62 fusion-negative, 23 of 23 PAX3-FOXO1 fusion-positive, and 8 of 8 PAX7-FOXO1 fusion-positive RMS, ≥3 standard deviations over the mean when compared to normal skeletal muscle, p=0.0009 for fusion-negative, p=0.0.0031 for PAX3-FOXO1, p=0.0011 for PAX7-FOXO1, Student's t-test comparison to normal muscle, Figure 1B). By contrast, VANGL1 was not differentially regulated in RMS when compared with normal muscle (Figure 1A). *VANGL2* was also highly expressed in an independent cohort of 12 primary patient samples when assessed by quantitative RT-PCR ($p<0.05$, Student's t-test, Figure 1C) and high protein levels were detected in a panel of human ERMS and ARMS cell lines (Figure 1D). IHC staining of pediatric RMS samples revealed VANGL2 was expressed in the majority of primary patient ERMS and ARMS (n=43/55 ERMS and n=14/18 ARMS, Figure 1E,F, Figure S1A,B). VANGL2 was detected in less than 10% of RMS cells in most cases (n=39/55 ERMS and n=13/18 ARMS, Figure 1E,F, Figure S1A,B), suggesting rarity of VANGL2+ cells and an underlying functional heterogeneity based on expression of this marker. VANGL2 expression was also confined to a fraction of sarcoma cells within Wilm's tumor, Synovial Sarcoma, and Desmoplastic small round cell tumor (TA-23, Stanford University Medical Centre, Figure S1C). Together, these data prompted us to further investigate VANGL2 in the context of tumor cell growth and TPC function.

VANGL2 affects growth and differentiation of human RMS

To assess the functional significance of VANGL2 in human RMS, *VANGL2* was knocked down using two short hairpin RNAs in PAX3-FOXO1 fusion positive ARMS (Rh30) and fusion negative ERMS (RD) cells (>90% knockdown, Figure 2A,E). By three days post infection, Rh30 and RD cells depleted of VANGL2 exhibited a large, rounded morphology compared to the characteristic spindle shape observed in shSCRAMBLE (shSCRM)-infected cells (Figure 2B,F). Nuclei counts revealed that loss of VANGL2 significantly inhibited RMS growth *in vitro* (Figure 2C,G). Analysis of EDU-incorporation by flow cytometry showed significant inhibition of cell proliferation with a >7-fold reduction in S-phase cycling cells following knock-down of VANGL2 at 72 hours (Figure 2D,H, $p<0.0001$, Student's t-test). This data showed that VANGL2 is required for human RMS tumor growth, acting predominantly through regulation of cell proliferation.

Human RD ERMS cells differentiate along a developmental hierarchy similar to that which occurs during myogenesis and regeneration (Keller and Guttridge, 2013). To test the effect of VANGL2 loss on RMS differentiation, we next assessed myogenic regulatory factors that are expressed at specific stages of muscle differentiation. Compared to control shSCRM-infected cells, VANGL2 knock-down led to a dramatic decrease in the expression of genes associated with progenitor-like cells including *PAX3, PAX7* and *MET* (Figure 2I, $p<0.01$, Student's t-test). Conversely, markers of differentiation were significantly up-regulated following VANGL2 knockdown, including *MCAD, MYOD* and *MYOG* (Figure 2I, $p<0.01$, Student's t-test). Differences in PAX7 and MYOG protein expression were confirmed by Western blot analysis (Figure 2E), and immunofluoresence, with these latter experiments revealing a significant decrease in PAX7 at the cellular level in VANGL2-depleted cells (Figure 2J-L, $p<0.001$, Student's t-test). Moreover, a dramatic increase in the overall number

of differentiated MYOG-positive cells was observed following VANGL2 depletion (Figure 2J,L, $p<0.001$, Student's t-test). These data are consistent with VANGL2 having important roles in maintenance of progenitor-like cell fates in human RMS.

Next, we assessed a role for *VANGL2* in growth and differentiation of human RMS *in vivo* using engraftment of control and VANGL2-depleted RD ERMS, SMSCTR ERMS, and Rh30 ARMS cells into the flanks of NOD/SCID/*IL2R*γ-null (NSG) female mice. Cells were labeled with firefly luciferase and engrafted animals were imaged weekly to observe differences in tumor growth over time (Figure 3A,B, Figure S2). Tumors derived from VANGL2-depleted cells displayed inhibition of growth by 28 days when monitored by total body luciferase imaging (Figure 3C-E, $p<0.001$ for RD and Rh30, $p=0.03$ for SMSCTR compared to shSCRM, Student's t-test). This was in contrast to shSCRM-infected control tumor cells, which increased >30 fold (Figure 3A-E, $p<0.01$, Student-t-test). At necropsy, 6 of 12 VANGL2-depleted RD-derived tumors and 7 of 12 VANGL2-depleted SMSCTR-derived tumors had fully regressed (Figure S2C,I). The remaining VANGL2-depleted ERMS tumors were significantly smaller and weighed less than controls (Figure S2D,E,J,K, $p<0.001$, Student's t-test). Excised tumors derived from VANGL2-depleted RD cells also exhibited reduced cellularity compared to controls (Figure 3F,K,P). Ki67 staining also revealed fewer proliferative cells in VANGL2 knock-down RD and SMSCTR ERMS tumors when compared to shSCRM-infected controls (Figure 3G,L,Q, Figure S2M,Q, $p<0.001$, Student's t-test), while tumors displayed no significant increase in cleaved caspase 3 (CC3) (Figure 3H,M,R, Figure S2N,R). In addition, both RD and SMSCTR VANGL2-depleted cells displayed dramatic increases in the number of differentiated RMS cells when assessed by IHC for MYOD (Figure 3I,N,S, $p<0.001$, Student's t-test) and MYOG (Figure 3J,O,T; Figure S2O,S, $p<0.001$, Student's t-test), further supporting a role for VANGL2 in the maintenance of ERMS progenitor cell fate.

In contrast to the xenograft studies using human ERMS, Rh30 ARMS tumors regrew after near complete tumor loss when assessed by luciferase bioluminescent imaging at 28 days (Figure 3E). Knockdown and control mice had similar sized tumors at necropsy by 60 days post engraftment (Figure S2V-X). IHC staining showed that Rh30-derived tumors that grew out lacked the lentiviral vector and regained VANGL2 expression equal to or greater than shSCRM-infected control cells (Figure S2Z). These data suggest that late-stage emergence of Rh30 ARMS resulted from growth of rare, uninfected cells introduced at the time of injection. Together, our results show that VANGL2 has important roles in regulating tumor growth and maintenance *in vivo* for both ERMS and ARMS.

VANGL2 is expressed in proliferating progenitor-like cells in human RMS

To characterize VANGL2 expression within heterogeneous cell types in RMS, human RD and Rh30 cells were assessed by immunofluorescence and co-stained with makers of proliferation and myogenic cell state. Confocal microscopy revealed that only a fraction of human RMS cells expressed VANGL2 (Figure 4A). Notably, the majority of VANGL2 expressing cells were actively dividing when assessed by Dapi and Ki67 staining (Figure 4B-K). This was in contrast to cells expressing low levels of VANGL2, which were largely non-mitotic (Figure 4J,K, $p<0.001$, Student's t-test). At the subcellular level, VANGL2 localized to the poles of cellular doublets in telophase (Figure 4G-I), consistent with observations made during development where Vangl2 localizes to opposite ends of the axis in polarized, actively-dividing satellite cells (Le Grand et al., 2009). Moreover, co-staining revealed that >80% of VANGL2+ cells co-expressed high levels of PAX7 (Figure 4A-D), a marker of progenitor cell fate in muscle (Buckingham and Relaix, 2015). Interestingly, VANGL2+ cells also expressed the highest levels of FGFR3 and CD133 (Figure 4L,M, Figure S3). These markers have been

previously associated with progenitor-like properties in RMS cells (Hirotsu et al., 2009; Pressey et al., 2013; Walter et al., 2011), suggesting that VANGL2 may be both a marker of TPCs and be required for self-renewal.

Vangl2 is required for maintenance of TPCs in human RMS

Human RD, Ruch2 and Rh36 ERMS cells can be efficiently grown as 3D rhabdospheres, which are 100-fold more tumorigenic than adherent cells when xenografted into immune-deficient mouse models and upregulate genes associated with stemness (Walter et al., 2011). Thus, rhabdosphere colony formation assays have become a powerful tool to estimate self-renewal in a subset of human ERMS and to identify pathways required for TPC maintenance and growth (Chen et al., 2014; Satheesha et al., 2015). Western blot analysis displayed upregulation of VANGL2 in RD, Ruch2 and Rh36 rhabdospheres (Figure 4N-P), suggesting possible association between VANGL2 and TPCs in human ERMS. We next assessed the requirement for VANGL2 during rhabdosphere colony formation. Specifically, control shSCRM and shVANGL2-infected RD, Ruch2 and Rh36 cells were plated at limiting cell dilution in stem cell media and the number of colonies was quantified after 10-20 days of growth (Figure 4Q-Y). VANGL2 depletion led to a dramatic decrease in colony formation (Figure 4W-Y, $p<0.001$) and culturing VANGL2 knock-down cells for more than 30 days in stem cell media failed to identify outgrowth of colonies, indicating a major requirement for VANGL2 in regulating rhabdosphere formation and in the maintenance of human RMS TPCs. Interestingly, VANGL2 was also upregulated in Rh30 ARMS cells grown in sphere media and depletion similarly led to inhibition of rhabdosphere formation (Figure S7), suggesting an association between VANGL2 and sphere colony formation in RMS regardless of subtype.

Vangl2 increases TPCs in zebrafish ERMS

VANGL2 is uniquely expressed in human RMS progenitor-like cells, is required for maintenance of cellular identity, and is required for rhabdosphere colony formation (a surrogate for assessing TPC number and function *in vitro*), suggesting an important role for Vangl2 in growth and maintenance of less differentiated tumor propagating cells in human RMS. To identify oncogenic roles for Vangl2 in regulating the overall frequency of self-renewing TPCs, we next utilized a syngeneic zebrafish model of *kRASG12D*-induced ERMS and performed cell transplantation experiments to quantity differences in RMS that express only kRASG12D with those that transgenically co-express kRASG12D and Vangl2. Importantly, the zebrafish *kRASG12D*-induced ERMS shares molecular and histopathological features with human RMS and has become a valuable model to assess conserved pathways that regulate TPC function *in vivo* (Chen et al., 2014; Ignatius et al., 2017; Langenau et al., 2007; Tenente et al., 2017).

Zebrafish ERMS were generated to transgenically express kRASG12D and GFP with and without Vangl2. In these studies, transgenic expression was driven by the minimal 6.5kB *rag2* promoter, which drives expression in muscle progenitors due to uncovering a *myoD* enhancer site (Langenau et al., 2007). Tumor formation was observed as early as 15 days in both kRASG12D alone and kRASG12D + Vangl2 ERMS, with no overt differences in latency, penetrance, or tumor size (Figure S4). H&E staining confirmed similar histology between kRASG12D alone and Vangl2 expressing ERMS (Figure S4B,D). Together, our data suggest minimal effects of Vangl2 over-expression on tumor initiation.

Next, we tested the effect of Vangl2 on modulating the overall fraction of TPCs using limiting dilution cell transplantation into syngeneic zebrafish. Highly purified GFP+ ERMS cells were isolated and introduced into syngeneic transplant recipient animals at limiting dilution

(>90% purity and viability). Animals were followed for tumor onset for 90 days and TPC frequency quantified using the Extreme limiting dilution analysis (ELDA) program. From these experiments, we observed an increase in overall engraftment rates of ERMS cells that transgenically expressed both kRASG12D and Vangl2 (28/67 total engrafted tumors from n=3 independent kRASG12D ERMS and 43/65 total engrafted tumors from n=3 independent kRASG12D + Vangl2 ERMS, p=0.004 Fisher Exact Test, Figure 5A-F). ELDA revealed a 9-fold increase in TPCs in kRASG12D + Vangl2 ERMS (Figure 5E,F, Table S1, $p<0.001$, ELDA). Transgenic expression of Vangl2 also led to significant down-regulation of markers associated with muscle differentiation including *myod* and *myog* (n=3 tumors analyzed/genotype, Figure 5G, $p<0.01$, two-way ANOVA). GFP-positive ERMS tumor cells did not have significant differences in *myf5* or *c-met* expression (Figure 5G), suggesting a role for Vangl2 in regulating TPC fate by specifically inhibiting cellular differentiation.

Vangl2 expression identifies self-renewing TPCs in zebrafish ERMS

A molecularly-defined tumor-propagating cell has been identified in zebrafish ERMS (Ignatius et al., 2012; Langenau et al., 2007). This self-renewing TPC expresses satellite cell markers including *myf5* and *c-met* and can be isolated using fluorescent protein expressed under control of muscle transgenic promoters that define specific cell states (Ignatius et al., 2012). For example, ERMS TPCs can be enriched using the *myf5*:GFP and *mylz2*:mCherry transgenic reporter lines, with GFP+/mCherry-negative cells exhibiting a >25-fold enrichment for TPCs when compared with more differentiated ERMS cells (Ignatius et al., 2012). Building on these findings, we first assessed if *vangl2* was expressed in specific kRASG12D-induced ERMS cell sub-populations. As expected based on co-expression of VANGL2 and progenitor cell markers in human RMS cells, endogenous *vangl2* was highly expressed in

myf5:GFP^{+}/*mylz2*:mCherry^{-} TPCs when compared with more differentiated *myf5*:GFP^{+}/*mylz2*:mCherry^{+} cells ($p<0.001$, Student's t-test, Figure S5A-C). *vangl2* was also expressed in differentiated *myf5*:GFP^{-}/*mylz2*:mCherry^{+} ERMS cells (Figure S5A-C), a pattern consistent with a developmental role for Wnt/PCP signaling in polarizing orientation of differentiated myofibers (Gros et al., 2009) and likely unrelated to self-renewal of ERMS TPCs.

To assess if *vangl2* expression enriches specifically for TPCs in the zebrafish model, we next utilized a transgenic labeling strategy where mCherry was expressed under the control of the *vangl2(-5kb)* promoter (*vangl2*:mCherry) (Sittaramane et al., 2013). This *vangl2* promoter drives at near endogenous levels and has been previously used to dynamically visualize Wnt/PCP-dependent developmental processes *in vivo* (Roszko et al., 2015; Sittaramane et al., 2013). CG1-strain syngeneic zebrafish were injected at the one cell stage with *rag2*:kRASG12D, *rag2*:GFP and *vangl2*:mCherry transgenes (Figures S6A,B). Following tumor expansion into syngeneic recipient fish (Figure S6C,D), fluorescent-labeled ERMS cell fractions were purified by FACS (n= 3 tumors/genotype, >90% viability and 80-95% purity, Figure S6E,F) and transplanted into syngeneic recipient animals at limiting dilution (Figure S6G-K, Table S2). *rag2*:GFP+/*vangl2*:mCherry+ double-positive cells displayed robust engraftment and propagated ERMS with a TPC frequency of 1 in 288 cells (180-461, 95% confidence interval, Figure S6K, Table S2). By contrast, ERMS cells that expressed only *rag2:*GFP propagated tumors far less efficiently with only 1 in >2218 cells able to induce tumor formation in the transplantation setting (Figure S6J,K, Table S2, $p<0.0001$, ELDA). FACS analysis also revealed a subpopulation of mature *vangl2*:mCherry single-positive cells that failed to engraft in recipient animals (Figure S6J,K), consistent with previous observations that tumor propagating ability is limited to less-mature *rag2*:GFP+ positive ERMS cell subpopulations (Langenau et al., 2007).

To determine if *vangl2*:mCherry expression further enriches for ERMS tumor propagating ability over the previously characterized *myf5*:GFP+ transgenic reporter (Ignatius et al., 2012), we next performed limiting dilution cell transplantation experiments using sorted *myf5*:GFP/*vangl2*:mCherry cells from four independent zebrafish ERMS (Figure 6, Table S3). When transplanted at limiting dilution into CG1 syngeneic recipient animals, *myf5*:GFP+/*vangl2*:mCherry+ cells efficiently propagated ERMS with an average TPC frequency of 1 in 59.6 and significantly enriched for tumor propagating ability 9-fold when compared to *myf5*:GFP+/*vangl2*:mCherry- cells (Figure 6I,J, Table S3, $p<0.0001$, ELDA). Only 1 in 519 *myf5*:GFP+/*vangl2*:mCherry- cells propagated ERMS in syngeneic recipient fish (Figure 6I,J, Table S3). Finally, *myf5*:GFP-/*vangl2*:mCherry+ cells did not propagate ERMS, consistent with TPCs being confined to less mature *myf5*:GFP+ ERMS cell subpopulations (Figure 6I,J, Table S3) (Ignatius et al., 2012). Together, these data reveal *vangl2*:mCherry expression as a refined marker of self-renewing ERMS TPCs *in vivo* that further enriches for engraftment potential over all previously characterized *in vivo* markers of TPCs.

To validate the long-term tumor-propagating potential of *vangl2*:mCherry+ cells, tumor cell populations were isolated from host animals and serially engrafted following FACS and limiting dilution cell transplantation. In all cases, purified *rag2*:GFP+/*vangl2*:mCherry+ or *myf5*:GFP+/*vangl2*:mCherry+ TPCs retained long-term engraftment potential (Figure S5E-H, S6L-O, Table S2 and S3). Histological analysis of serially passaged tumors revealed similar morphology as primary and early passaged ERMS tumors (Figure S5G, S6N). FACS confirmed that serially passaged tumors were capable of regenerating all cellular subpopulations in zebrafish ERMS, which was independently confirmed by qRT-PCR performed on sorted ERMS cell subfractions (Figure 6K). *myf5*:GFP+/*vangl2*:mCherry+ TPCs expressed the satellite cell markers *myf5* and *c-met* and additional markers associated with human RMS TPCs including *fgfr1a* and *fgfr3* (Figure 6K, Figure S5I) (Armand et al., 2003;

Goldstein et al., 2007; Hirotsu et al., 2009). By contrast, *myf5*:GFP+/*vangl2*:mCherry- cells were more differentiated and expressed higher levels of *myog*, *mylz2*, *troponin I fast-twitch isoform 2 (tnni2a)* and *α-actin 1b (acta1b)* (Figure 6K, $p<0.01$, Student's t-test). Finally, differentiated *myf5*:GFP-/*vangl2*:mCherry+ cells expressed the most mature muscle markers including *actin-related protein 2/3 complex subunit 5b (arpc5b)* and *myosin heavy chain 9a (myh9a)* (Figure 6K, $p<0.001$, Student's t-test), consistent with the observation that these cells do not propagate ERMS and likely represent a subpopulation of non-proliferative and terminally differentiated ERMS cells (Ignatius et al., 2012; Langenau et al., 2007). Our analysis shows that *myf5*:GFP+/*vangl2*:mCherry+ ERMS cells are enriched for molecular markers associated with TPCs and retain long-term self-renewal properties, further defining *vangl2*:mCherry as a marker of ERMS TPCs *in vivo*.

RHOA regulates TPC growth and maintenance downstream of VANGL2 in human RMS

We next wanted to identify pathways downstream of VANGL2 that modulate human RMS growth and TPC function. Because Wnt/PCP signaling typically relies on activation of the Rho-family GTPases RHOA and RAC1 (Schlessinger et al., 2009), we first assessed their expression in adherent and 3D rhabdosphere cells. We observed increased RHOA in RD ERMS, Rh36 ERMS and Rh30 ARMS rhabdosphere culture compared to adherent cells, coincident with upregulation of VANGL2 (Figure 7A,E, Figure S7A). By contrast, RAC1 protein was not consistently differentially regulated across cell lines in adherent and rhabdosphere growth conditions (Figure S7A,L,O), suggesting a limited role for RAC1/JNK signaling in regulating TPC function.

To investigate RHOA activity downstream of VANGL2, we next assessed total RHOA and activated GTP-bound RHOA in control and VANGL2 knockdown RD, Rh36 and Rh30

cells (Figure 7B,F, S7H). Interestingly, we observed reductions of total and activated forms of RHOA in VANGL2-depleted RMS cells (Figure 7B,F, S7H), suggesting RHOA is required downstream of VANGL2 to maintain TPCs and to elevate overall tumor propagating potential. Importantly, our results show that both RHOA activation and expression are modulated downstream of VANGL2, consistent with reports from other groups showing this duality of control by VANGL2 (Phillips et al., 2005). By contrast, activated GTP-bound RAC1 was not consistently differentially regulated following VANGL2 knockdown (Figure S7J,M,P).

We next performed epistasis experiments using constitutively-active and dominant-negative forms of RHOA and RAC1 and assessed restoration of RMS colony growth *in vitro.* Specifically, control and VANGL2-depleted RD ERMS, Rh36 ERMS and Rh30 ARMS cells were infected with constitutively-active ($RHOA^{V14}$, $RAC1^{V12}$) or dominant-negative ($RHOA^{N19}$, $RAC1^{N17}$) forms of human RHOA or RAC1 and assessed in rhabdosphere colony formation assays (Figure 7C,G, Figure S7). Constitutively-active $RHOA^{V14}$ stimulated rhabdosphere colony formation in control cells ($p<0.01$ for RD and Rh36, $p=0.033$ for Rh30, Figure 7C,G, Figure S7D,I) while dominant-negative $RHOA^{N19}$ reduced rhabdosphere formation (Figure 7C,G, Figure S7F,I, $p<0.05$, Student's t-test). $RHOA^{V14}$ also rescued rhabdosphere colony formation in VANGL2-depleted RMS cells ($p<0.001$, Figure 7C,G, Figure S7E,I, $p<0.01$, Student's t-test), while dominant-negative $RHOA^{N19}$ failed to rescue rhabdosphere formation (Figure 7C,G, Figure S7G,I). By contrast, neither constitutively-active $RAC1^{V12}$ or dominant-negative $RAC1^{N17}$ could restore colony formation to VANGL2-depleted cultures (Figure S7K,N,Q). Together, these data support a role for RHOA signaling downstream of VANGL2 in human RMS.

Finally, to investigate the effect of RHOA signaling on RMS TPCs and regulation of their differentiation, we next assessed myogenic factor expression in RD control, VANGL2-depleted, and $RHOA^{V14}$ expressing cells. As expected, cells depleted of VANGL2 exhibited

significant increases in the expression of differentiated muscle gene transcripts when compared with control cells (Figure 7D) while constitutively-active $RHOA^{V14}$ blocked differentiation and retained ERMS cells in a more undifferentiated, self-renewing TPC fate (Figure 7D). Together these data show that RHOA acts downstream of VANGL2 to maintain progenitor-like cell fates in ERMS and modulates the overall numbers of TPCs in human RMS. These functional studies reveal roles for a VANGL2/RHOA signaling axis in regulating sustained tumor growth through maintenance of self-renewing cell divisions.

Discussion

Stem cells have the capacity to self-renew and generate more of themselves, yet these cells can also differentiate into specialized cells with unique functional characteristics. Despite a large body of literature supporting roles for canonical Wnt/β-catenin signaling in regulating stemness and cellular fate (Nusse and Clevers, 2017), alternative Wnt signaling pathways including non-canonical Wnt/PCP signaling are less well understood. Factors associated with non-canonical Wnt signaling pathways are elevated in a large number of human cancers and are linked to poor outcome (Anastas et al., 2012; Asad et al., 2014; Gujral et al., 2014; Ma et al., 2014; Puvirajesinghe et al., 2016; Weeraratna et al., 2002; Yagyu et al., 2002; Yang et al., 2015). VANGL proteins are required for tumor cell proliferation and growth in hepatocellular carcinoma and basal cell breast cancer (Puvirajesinghe et al., 2016; Yagyu et al., 2002) while other functional studies have focused on the role for VANGL proteins and Rho-GTPases in tumor cell invasion and metastasis (Anastas et al., 2012; Asad et al., 2014; Kurayoshi et al., 2006; Ma et al., 2014; Weeraratna et al., 2002; Yang et al., 2015). These features are consistent with known roles for this pathway in regulating migration during normal tissue morphogenesis (Seifert and Mlodzik, 2007; Simons and Mlodzik, 2008). To date, no reports

have identified specific roles for the Wnt/PCP pathway in regulating TPC growth, maintenance, or self-renewal. Our work has identified a role for Vangl2 in the maintenance of tumor progenitor cells in both human and zebrafish rhabdomyosarcoma. Moreover, our work shows that *Vangl2* labels early ERMS progenitor cells and enriches for tumor propagating cells (TPCs) in both zebrafish and human, thus identifying a cross-species marker of ERMS stem-like subpopulations. Our work also revealed a requirement for VANGL2 in regulating growth, colony formation, and *in vivo* tumor maintenance in both human ERMS and ARMS, suggesting that conserved self-renewal properties may underlie RMS regardless of subtype and encourage future exploration of the relationship between VANGL2 and TPCs in ARMS.

We have also uncovered a major role for RHOA in regulating proliferation and maintenance of cell fate in RMS downstream of VANGL2. Despite data implicating RhoA signaling in self-renewal of embryonic stem cells (Jaganathan et al., 2013; Lee et al., 2007; Xu et al., 2012), mechanistic requirements for RhoA during self-renewing cancer stem cell divisions are not well understood. Given that RhoA affects myoblast proliferation through direct transcriptional regulation of *MYOD* (Carnac et al., 1998; Dhawan and Helfman, 2004; Gopinath et al., 2007), and our recent discovery that *MYF5/MYOD* is required for growth and self-renewal in human RMS (Tenente et al., 2017), it will be important to define the relationship between VANGL2/RHOA, MYOD transcription factory family members, and proliferative programs that drive tumor growth in RMS. Wnt/PCP signaling is known to affect the orientation of cell divisions in normal tissue (Ciruna et al., 2006; Gong et al., 2004; Segalen and Bellaïche, 2009), and it will be interesting in the future to dynamically visualize RhoA-dependent mechanisms in malignant cells to understand how orientation of proliferating TPCs may influence subsequent cell fate decisions and cancer growth *in vivo*.

Our work also suggests that inhibiting the VANGL2-RHOA signaling axis may provide new strategies to specifically target RMS TPCs that drive relapse and metastatic growth.

Preclinical pharmacologic approaches have successfully inhibited non-canonical Wnt signaling in hepatocellular carcinoma, leading to a reduction in xenograft growth and metastasis (Gujral et al., 2014). As a consequence, several clinical trials are currently underway to test chemical or antibody-based therapeutics designed to target Wnt/PCP in several different forms of human cancer (Daulat and Borg, 2017). Several FDA approved small molecule inhibitors of RhoA have also been identified (Kopp et al., 2012; Lee et al., 2007). It will be important for future experiments to test these compounds for effects on RMS self-renewal and for preclinical efficacy in suppressing xenograft growth of human RMS, in addition to suppressing more commonly RhoA-associated activities including tumor cell invasion and metastasis.

Finally, we have previously uncovered similarities in pathways that regulate stemness in normal muscle growth, regeneration, and cancer. For example, we have identified important roles for intracellular NOTCH1 in regulating TPC self-renewal and number, while activation of the Wnt/β-catenin pathway induces TPC differentiation in rhabdomyosarcoma (Chen et al., 2014; Ignatius et al., 2017). It has been shown that the Wnt/PCP signaling pathway plays important roles in regulating self-renewal cell divisions in neuronal progenitor cells and muscle stem cells (Le Grand et al., 2009; Lake and Sokol, 2009). In regenerating muscle, Wnt7a induces the expansion of satellite cells through the non-canonical Wnt/PCP pathway (Le Grand et al., 2009). In this setting, Wnt7a signals through the Fz7a receptor to polarize distribution of Vangl2, resulting in the expansion of satellite cells and enhanced muscle regeneration. Loss of Vangl2 also led to increased muscle differentiation *in vivo* (Le Grand et al., 2009), akin to that seen following VANGL2 knockdown in human RMS. Despite some commonalities with our studies, the downstream effectors of VANGL2 responsible for direct regulation of stem cell self-renewal in muscle have not yet been identified nor have roles for VANGL2 in regulating expansion of highly proliferative stem cell pools been

established. Based on our findings and the remarkable conservation in stem cell programs between normal satellite cells and RMS, it is likely that Vangl2/RhoA will have a similar role in development and muscle regeneration.

In conclusion, we have described a role for Vangl2 in regulating the frequency and identity of tumor-sustaining cell types in RMS. Our work also suggests important and highly conserved roles for Wnt/PCP signaling in regulating cancer stem cell self-renewal across species and experimental platforms, raising the possibility that similar pathways exist in other tumor types and can be targeted therapeutically in the future (Daulat and Borg, 2017).

Acknowledgments: This work was funded by R01CA154923 (D.M.L), R01CA215118 (DML), R24OD016761 (D.M.L), U54CA168512 (D.M.L.), a St. Baldricks Research Grant (D.M.L), the Alex's Lemonade Stand Foundation (M.N.H), and the Amanda Riley Foundation (M.N.H., Bear Necessities). We thank the Specialized Histopathology Services at Massachusetts General Hospital (MGH) and the Dana-Farber/Harvard Cancer Center (P30 CA06516), the MGH Cancer Center/Molecular Pathology Confocal Core and the MGH CNY Flow Cytometry Core and Flow Image Analysis (1S10RR023440-01A1). Work of Z.M. and D.M. supported through a Rhabdomyosarcoma Research Fund from SickKids Foundation. Work of M.I. supported by R00CS175184.

Author Contributions: M.N.H. and D.M.L. conceptualized the study. M.N.H. designed and performed experiments. K.M., A.J., M.L.O. and M.S.I. assisted with experimental design and execution. S.I. and S.G. performed bioinformatics analysis. S.S., B.G., and J.K. provided patient RNAseq dataset and performed initial expression analysis. Z.M. and D.M. provided primary patient expression data and performed expression analysis. J-P.B. provided VANGL2 antibody. G.P.N. analyzed human IHC. M.vdR. provided human TMA. All authors discussed results and commented on the manuscript. D.M.L. supervised the project and oversaw the scientific direction.

References

Anastas, J.N., Biechele, T.L., Robitaille, M., Muster, J., Allison, K.H., Angers, S., and Moon, R.T. (2012). A protein complex of SCRIB, NOS1AP and VANGL1 regulates cell polarity and migration, and is associated with breast cancer progression. Oncogene *31*, 3696–3708.

Armand, A.S., Launay, T., Pariset, C., Della Gaspera, B., Charbonnier, F., and Chanoine, C. (2003). Injection of FGF6 accelerates regeneration of the soleus muscle in adult mice. Biochim. Biophys. Acta - Mol. Cell Res. *1642*, 97–105.

Asad, M., Wong, M.K., Tan, T.Z., Choolani, M., Low, J., Mori, S., Virshup, D., Thiery, J.P., and Huang, R.Y.-J. (2014). FZD7 drives in vitro aggressiveness in Stem-A subtype of ovarian cancer via regulation of non-canonical Wnt/PCP pathway. Cell Death Dis. *5*, e1346.

Belotti, E., Puvirajesinghe, T.M., Audebert, S., Baudelet, E., Camoin, L., Pierres, M., Lasvaux, L., Ferracci, G., Montcouquiol, M., and Borg, J.P. (2012). Molecular Characterisation of Endogenous Vangl2/Vangl1 Heteromeric Protein Complexes. PLoS One *7*.

Brack, A.S., Conboy, I.M., Conboy, M.J., Shen, J., and Rando, T.A. (2008). A Temporal Switch from Notch to Wnt Signaling in Muscle Stem Cells Is Necessary for Normal Adult Myogenesis. Cell Stem Cell *2*, 50–59.

Buckingham, M., and Relaix, F. (2015). PAX3 and PAX7 as upstream regulators of myogenesis. Semin. Cell Dev. Biol. *44*, 115–125.

Carnac, G., Primig, M., Kitzmann, M., Chafey, P., Tuil, D., Lamb, N., and Fernandez, A. (1998). RhoA GTPase and serum response factor control selectively the expression of MyoD without affecting Myf5 in mouse myoblasts. Mol. Biol. Cell *9*, 1891–1902.

Chen, E.Y., Deran, M.T., Ignatius, M.S., Grandinetti, K.B., Clagg, R., McCarthy, K.M., Lobbardi, R.M., Brockmann, J., Keller, C., Wu, X., et al. (2014). Glycogen synthase kinase 3 inhibitors induce the canonical WNT/β-catenin pathway to suppress growth and self-renewal in embryonal rhabdomyosarcoma. Proc. Natl. Acad. Sci. U. S. A. *111*, 5349–5354.

Chen, X., Stewart, E., Shelat, A., Qu, C., Bahrami, A., Hatley, M., Wu, G., Bradley, C., McEvoy, J., Pappo, A., et al. (2013). Targeting Oxidative Stress in Embryonal Rhabdomyosarcoma. Cancer Cell *24*, 710–724.

Chen, Y.-H., Wang, Y.-H., Chang, M.-Y., Lin, C.-Y., Weng, C.-W., Westerfield, M., and Tsai, H.-J. (2007). Multiple upstream modules regulate zebrafish myf5 expression. BMC Dev. Biol. *7*, 1.

Ciruna, B., Jenny, A., Lee, D., Mlodzik, M., and Schier, A.F. (2006). Planar cell polarity signalling couples cell division and morphogenesis during neurulation. Nature *439*, 220–224.
Dela Cruz, F.S. (2013). Cancer stem cells in pediatric sarcomas. Front. Oncol. *3*, 168.
Daulat, A.M., and Borg, J.-P. (2017). Wnt/Planar Cell Polarity Signaling: New Opportunities for Cancer Treatment. Trends in Cancer *3*, 113–125.

Dhawan, J., and Helfman, D.M. (2004). Modulation of acto-myosin contractility in skeletal

muscle myoblasts uncouples growth arrest from differentiation. J. Cell Sci. *117*, 3735–3748.
Friedman, G.K., and Gillespie, G.Y. (2011). Cancer stem cells and pediatric solid tumors. Cancers (Basel). *3*, 298–318.

Goldstein, M., Meller, I., and Orr-Urtreger, A. (2007). FGFR1 over-expression in primary rhabdomyosarcoma tumors is associated with hypomethylation of a 5′ CpG island and abnormal expression of the AKT1, NOG, and BMP4 genes. Genes Chromosom. Cancer *46*, 1028–1038.

Gong, Y., Mo, C., and Fraser, S.E. (2004). Planar cell polarity signalling controls cell division orientation during zebrafish gastrulation. Nature *430*, 689–693.

Gopinath, S.D., Narumiya, S., and Dhawan, J. (2007). The RhoA effector mDiaphanous regulates MyoD expression and cell cycle progression via SRF-dependent and SRF-independent pathways. J. Cell Sci. *120*, 3086–3098.

Le Grand, F., Jones, A.E., Seale, V., Scimè, A., and Rudnicki, M.A. (2009). Wnt7a activates the planar cell polarity pathway to drive the symmetric expansion of satellite stem cells. Cell Stem Cell *4*, 535–547.

Gros, J., Serralbo, O., and Marcelle, C. (2009). WNT11 acts as a directional cue to organize the elongation of early muscle fibres. Nature *457*, 589–593.

Gujral, T.S., Chan, M., Peshkin, L., Sorger, P.K., Kirschner, M.W., and Macbeath, G. (2014). A noncanonical frizzled2 pathway regulates epithelial-mesenchymal transition and metastasis. Cell *159*, 844–856.

Hirotsu, M., Setoguchi, T., Matsunoshita, Y., Sasaki, H., Nagao, H., Gao, H., Sugimura, K., and Komiya, S. (2009). Tumour formation by single fibroblast growth factor receptor 3-positive rhabdomyosarcoma-initiating cells. Br. J. Cancer *101*, 2030–2037.

Ignatius, M.S., Chen, E., Elpek, N.M., Fuller, A.Z., Tenente, I.M., Clagg, R., Liu, S., Blackburn, J.S., Linardic, C.M., Rosenberg, A.E., et al. (2012). In vivo imaging of tumor-propagating cells, regional tumor heterogeneity, and dynamic cell movements in embryonal rhabdomyosarcoma. Cancer Cell *21*, 680–693.

Ignatius, M.S., Hayes, M.N., Lobbardi, R., Chen, E.Y., McCarthy, K.M., Sreenivas, P., Motala, Z., Durbin, A.D., Molodtsov, A., Reeder, S., et al. (2017). The NOTCH1/SNAIL1/MEF2C Pathway Regulates Growth and Self-Renewal in Embryonal Rhabdomyosarcoma. Cell Rep. *19*, 2304–2318.

Jaganathan, B.G., Anjos-Afonso, F., Kumar, A., and Bonnet, D. (2013). Active RHOA favors retention of human hematopoietic stem/progenitor cells in their niche. J. Biomed. Sci. *20*, 66.

Jessen, J.R., Jessen, T.N., Vogel, S.S., and Lin, S. (2001). Concurrent expression of recombination activating genes 1 and 2 in zebrafish olfactory sensory neurons. Genesis *29*, 156–162.

Keller, C., and Guttridge, D.C. (2013). Mechanisms of impaired differentiation in

rhabdomyosarcoma. FEBS J. *280*, 4323–4334.

Kopp, M.A., Liebscher, T., Niedeggen, A., Laufer, S., Brommer, B., Jungehulsing, G.J., Strittmatter, S.M., Dirnagl, U., and Schwab, J.M. (2012). Small-molecule-induced Rho-inhibition: NSAIDs after spinal cord injury. Cell Tissue Res. *349*, 119–132.

Kreso, A., and Dick, J.E. (2014). Evolution of the cancer stem cell model. Cell Stem Cell *14*, 275–291.

Kurayoshi, M., Oue, N., Yamamoto, H., Kishida, M., Inoue, A., Asahara, T., Yasui, W., and Kikuchi, A. (2006). Expression of Wnt-5a is correlated with aggressiveness of gastric cancer by stimulating cell migration and invasion. Cancer Res. *66*, 10439–10448.

Lake, B.B., and Sokol, S.Y. (2009). Strabismus regulates asymmetric cell divisions and cell fate determination in the mouse brain. J. Cell Biol. *185*, 59–66.

Langenau, D.M., Keefe, M.D., Storer, N.Y., Guyon, J.R., Kutok, J.L., Le, X., Goessling, W., Neuberg, D.S., Kunkel, L.M., and Zon, L.I. (2007). Effects of RAS on the genesis of embryonal rhabdomyosarcoma. Genes Dev. *21*, 1382–1395.

Langenau, D.M., Keefe, M.D., Storer, N.Y., Jette, C.A., Smith, A.C.H., Ceol, C.J., Bourque, C., Look, A.T., and Zon, L.I. (2008). Co-injection strategies to modify radiation sensitivity and tumor initiation in transgenic Zebrafish. Oncogene *27*, 4242–4248.

Lee, M.-H., Cho, Y.S., and Han, Y.-M. (2007). Simvastatin suppresses self-renewal of mouse embryonic stem cells by inhibiting RhoA geranylgeranylation. Stem Cells *25*, 1654–1663.

Ma, M.Z., Zhuang, C., Yang, X.M., Zhang, Z.Z., Ma, H., Zhang, W.M., You, H., Qin, W., Gu, J., Yang, S., et al. (2014). CTHRC1 acts as a prognostic factor and promotes invasiveness of gastrointestinal stromal tumors by activating Wnt/PCP-Rho signaling. Neoplasia (United States) *16*, 265–278.

von Maltzahn, J., Chang, N.C., Bentzinger, C.F., and Rudnicki, M.A. (2012). Wnt signaling in myogenesis. Trends Cell Biol. *22*, 602–609.

Mccoy, K.E., Zhou, X., and Vize, P.D. (2011). Non-canonical wnt signals antagonize and canonical wnt signals promote cell proliferation in early kidney development. Dev. Dyn. *240*, 1558–1566.

Mizgireuv, I. V., and Revskoy, S.Y. (2006). Transplantable tumor lines generated in clonal zebrafish. Cancer Res. *66*, 3120–3125.

Murdoch, J.N. (2001). Severe neural tube defects in the loop-tail mouse result from mutation of Lpp1, a novel gene involved in floor plate specification. Hum. Mol. Genet. *10*, 2593–2601.

Nemeth, M.J., Topol, L., Anderson, S.M., Yang, Y., and Bodine, D.M. (2007). Wnt5a inhibits canonical Wnt signaling in hematopoietic stem cells and enhances repopulation. Proc. Natl. Acad. Sci. U. S. A. *104*, 15436–15441.

Nusse, R., and Clevers, H. (2017). Wnt/β-Catenin Signaling, Disease, and Emerging Therapeutic Modalities. Cell *169*, 985–999.

Peng, Y., and Axelrod, J.D. (2012). Asymmetric protein localization in planar cell polarity: mechanisms, puzzles, and challenges. Curr. Top. Dev. Biol. *101*, 33–53.

Phillips, H.M., Murdoch, J.N., Chaudhry, B., Copp, A.J., and Henderson, D.J. (2005). Vangl2 acts via RhoA signaling to regulate polarized cell movements during development of the proximal outflow tract. Circ. Res. *96*, 292–299.

Pressey, J.G., Haas, M.C., Pressey, C.S., Kelly, V.M., Parker, J.N., Gillespie, G.Y., and Friedman, G.K. (2013). CD133 marks a myogenically primitive subpopulation in rhabdomyosarcoma cell lines that are relatively chemoresistant but sensitive to mutant HSV. Pediatr. Blood Cancer *60*, 45–52.

Puvirajesinghe, T.M., Bertucci, F., Jain, A., Scerbo, P., Belotti, E., Audebert, S., Sebbagh, M., Lopez, M., Brech, A., Finetti, P., et al. (2016). Identification of p62/SQSTM1 as a component of non-canonical Wnt VANGL2–JNK signalling in breast cancer. Nat. Commun. *7*, 10318.

Roszko, I., S. Sepich, D., Jessen, J.R., Chandrasekhar, a., and Solnica-Krezel, L. (2015). A dynamic intracellular distribution of Vangl2 accompanies cell polarization during zebrafish gastrulation. Development *142*, 2508–2520.

Satheesha, S., Manzella, G., Bovay, A, Casanova, E.A., Bode, P.K., Belle, R., Feuchtgruber, S., Jaaks, P., Dogan, N., Koscielniak, E., et al. (2015). Targeting hedgehog signaling reduces self-renewal in embryonal rhabdomyosarcoma. Oncogene 1–11.

Schlessinger, K., Hall, A., and Tolwinski, N. (2009). Wnt signaling pathways meet Rho GTPases. Genes Dev. *23*, 265–277.

Segalen, M., and Bellaïche, Y. (2009). Cell division orientation and planar cell polarity pathways. Semin. Cell Dev. Biol. *20*, 972–977.

Seifert, J.R.K., and Mlodzik, M. (2007). Frizzled/PCP signalling: a conserved mechanism regulating cell polarity and directed motility. Nat. Rev. Genet. *8*, 126–138.

Shern, J.F., Chen, L., Chmielecki, J., Wei, J.S., Patidar, R., Rosenberg, M., Ambrogio, L., Auclair, D., Wang, J., Song, Y.K., et al. (2014). Comprehensive genomic analysis of rhabdomyosarcoma reveals a landscape of alterations affecting a common genetic axis in fusion-positive and fusion-negative tumors. Cancer Discov. *4*, 216–231.

Simons, M., and Mlodzik, M. (2008). Planar cell polarity signaling: from fly development to human disease. Annu. Rev. Genet. *42*, 517–540.

Sittaramane, V., Pan, X., Glasco, D.M., Huang, P., Gurung, S., Bock, A., Li, S., Wang, H., Kawakami, K., Matise, M.P., et al. (2013). The PCP protein Vangl2 regulates migration of hindbrain motor neurons by acting in floor plate cells, and independently of cilia function. Dev. Biol. *382*, 400–412.

Smith, A.C.H., Raimondi, A.R., Salthouse, C.D., Ignatius, M.S., Blackburn, J.S., Mizgirev, I. V., Storer, N.Y., De Jong, J.L.O., Chen, A.T., Zhou, Y., et al. (2010). High-throughput cell transplantation establishes that tumor-initiating cells are abundant in zebrafish T-cell acute lymphoblastic leukemia. Blood *115*, 3296–3303.

Tenente, I.M., Hayes, M.N., Ignatius, M.S., McCarthy, K., Yohe, M., Sindiri, S., Gryder, B., Oliveira, M.L., Ramakrishnan, A., Tang, Q., et al. (2017). Myogenic regulatory transcription factors regulate growth in rhabdomyosarcoma. Elife *6*, 1–24.

Walter, D., Satheesha, S., Albrecht, P., Bornhauser, B.C., D'Alessandro, V., Oesch, S.M., Rehrauer, H., Leuschner, I., Koscielniak, E., Gengler, C., et al. (2011). CD133 positive embryonal rhabdomyosarcoma stem-like cell population is enriched in rhabdospheres. PLoS One *6*: e19506.

Weeraratna, A.T., Jiang, Y., Hostetter, G., Rosenblatt, K., Duray, P., Bittner, M., and Trent, J.M. (2002). Wnt5a signaling directly affects cell motility and invasion of metastatic melanoma. Cancer Cell *1*, 279–288.

Xu, J., Lim, S.B.H., Ng, M.Y., Mohamed Ali, S., Kausalya, J.P., Limviphuvadh, V., Maurer-Stroh, S., and Hunziker, W. (2012). ZO-1 regulates Erk, Smad1/5/8, Smad2, and RhoA activities to modulate self-renewal and differentiation of mouse embryonic stem cells. Stem Cells *30*, 1885–1900.

Xu, Y., He, J., Tian, H.L., Chan, C.H., Liao, J., Yan, T., Lam, T.J., and Gong, Z. (1999). Fast skeletal muscle-specific expression of a zebrafish myosin light chain 2 gene and characterization of its promoter by direct injection into skeletal muscle. DNA Cell Biol. *18*, 85–95.

Yagyu, R., Hamamoto, R., Furukawa, Y., Okabe, H., Yamamura, T., and Nakamura, Y. (2002). Isolation and characterization of a novel human gene, VANGL1, as a therapeutic target for hepatocellular carcinoma. Int. J. Oncol. *20*, 1173–1178.

Yang, X.-M., You, H.-Y., Li, Q., Ma, H., Wang, Y.-H., Zhang, Y.-L., Zhu, L., Nie, H.-Z., Qin, W.-X., Zhang, Z.-G., et al. (2015). CTHRC1 promotes human colorectal cancer cell proliferation and invasiveness by activating Wnt/PCP signaling. Int. J. Clin. Exp. Pathol. *8*, 12793–12801.

Figure Legends

Figure 1. VANGL2 is highly expressed in human RMS subtypes. (A) Normalized expression (FPKM) for Wnt/PCP-associated genes from RNA sequencing of normal muscle, fusion-negative (FUS NEG) and fusion-positive (FUS POS) RMS samples. Each datum point represents an individual sample. The mean expression is noted by a horizontal bar with significance denoted by asterisks (*p<0.01, n.s. not significant, Student's t-test). (B) Normalized expression data (FPKM) depicting *Van Gogh-like 2* (*VANGL2*) in normal muscle, fusion-negative, PAX3-FOXO1 and PAX7-FOXO1 patient samples (p=0.0009 for fusion-negative, p=0.0.0031 for PAX3-FOXO1, p=0.0011 for PAX7-FOXO1, Student's t-test comparison to normal muscle). (C) Quantitative real-time PCR analysis of *VANGL2* in an independent cohort of normal muscle, RMS cell lines (RD, Rh18, Rh6), fusion-negative, and fusion-positive patient RMS samples (p<0.05 for all samples, relative to muscle). (D) Western blot analysis of human RMS cell lines. GAPDH is used as a loading control. (E) Immunohistochemistry showing VANGL2 and hematoxylin and eosin (H&E) stained sections of representative primary human ERMS and ARMS. Arrowheads highlight VANGL2+ cells. Scale bar is 100μm. (F) Quantification of the percentage of VANGL2+ cells found in primary ERMS and ARMS.

Figure 2. VANGL2 is required for growth of human RMS cells. (A-D) Phenotypic analysis for Rh30 fusion-positive ARMS cells. (A) Western blot analysis following scramble shRNA (shSCRM) and VANGL2 shRNA (shVL2(1), shVANGL2(2)) knockdown. GAPDH is used as a loading control. (B) Bright-field images of Rh30 cells at 4 days post infection. VANGL2 knock-down cells with prominent rounded cellular morphology are denoted (black arrow). Scale bar is 10μm. (C) Cell counts performed at 24 and 48 hours post plating equal numbers of shRNA-

infected cells (24 hours post infection). Cell number is normalized to 0 hours. (D) EdU and Propidium Iodide (PI) flow cytometry analysis of cell cycle in Rh30 cells at 4 days post infection. (E-L) Phenotypic analysis of RD fusion-negative ERMS cells. (E) Western blot analysis for VANGL2, PAX7 and MYOG protein expression in shSCRM and shVL2-infected RD cells. GAPDH is used as a loading control. (F) Bright-field images of RD cells after 4 days post infection with rounded cellular morphology denoted by black arrow. Scale bar is 10μm . (G) RD cell counts performed at 24 and 48 hours post plating equal numbers of shRNA-infected cells (24 hours post infection). Cell number is normalized to 0 hours. (H) EdU and Propidium Iodide (PI) flow cytometry analysis of cell cycle in RD cells 4 days post infection. (I) Quantitative real-time PCR gene expression analysis of muscle progenitor genes *PAX3, PAX7,* and *MET,* and differentiated genes *M-CADHERIN* (*MCAD), MYOD,* and *MYOGENIN (MYOG)*. (J) Immunofluorescence staining for PAX7 (red) and MYOG (green) in scramble shRNA (shSCRM) and VANGL2 shRNA-infected RD cells. (K) Quantification of cellular PAX7 fluorescent intensity in shRNA treated RD cells. (L) Quantification of MYOG-positive cells. *p<0.05, **p<0.01, ***p<0.001, Student's t-test. Error bars represent standard deviation.

Figure 3. *VANGL2* is required for xenograft growth and inhibits tumor cell differentiation *in vivo*. (A,B) Luciferase bioluminescent imaging of mice engrafted with bulk RD cells infected with scramble shRNA (left, scr) or VANGL2 shRNAs (right, shVL2). Representative animals are shown immediately after injection (A, 0 days) and 28 days post injection (B). (C-E) Quantification of tumor size based on bioluminescence relative to day 0 for (C) RD, (D) SMSCTR, and (E) Rh30 xenograft experiments infected with scramble shRNA (shSCRM) or VANGL2 shRNAS (shVL2(1) and shVL2(2)). n ≥ 6 animals/arm. Experiments shown for SMSCTR were completed on different days with control shSCRM results compiled across experiments. Independent shSCRM experiments are shown in Figure S2. (F-O)

Histological characterization of scramble (F-J) and VANGL2 shRNA-infected RD xenografted tumors (K-O). Representative images of hematoxylin and eosin stained sections (F,K), IHC for Ki67 (G,L), cleaved caspase 3 (CC3, H,M), MYOD (I,N), and MYOG (J,O). (P) Quantification of nuclei counts/tumor area. (Q) Percentage of Ki67 positive cells within tumors. (R) Percentage of ERMS cells that stained for activated caspase 3 (CC3). Quantification of immunohistochemical analysis for MYOD (S) and MYOG (T). *p<0.05, **p<0.01, ***p<0.001, n.s. not significant, Student's t-test. Error bars represent standard deviation. Scale bar is 100μm.

Figure 4. VANGL2 is expressed in proliferating progenitor cells and is required for 3D rhabdosphere colony formation. (A-K) VANGL2 expressing cells express high levels of progenitor cell markers and are highly mitotic. (A-G) Immunofluorescent staining of VANGL2 and PAX7 in RD cells. VANGL2 is co-expressed with the PAX7 progenitor cell marker (white arrowhead in A). (B-D) High magnification image of the VANGL2+/PAX7+ cell denoted in A by arrow. (E-G) Representative images of VANGL2+/PAX7+ cells undergoing mitotic division. (H,I) VANGL2 and Ki67 staining in RD (H) and Rh30 (I) cells. (J,K) Correlation of PAX7 and mitosis in VANGL2-high versus VANGL2-low expressing RD (J) and RH30 (K) cells. (L,M) VANGL2 is co-expressed with FGFR3 (L) and CD133 (M) in human RD cells. Merged and single fluorescent channel images are shown. (N-P) VANGL2 is highly expressed in 3D rhabdosphere culture as assessed by Western blot analysis for RD (N), Ruch2 (O) and Rh36 (P). (Q-V) Rhabdospheres stably expressing scramble shRNA (shSCRM) or VANGL2 shRNA (shVL2) shown at 10 for RD and Ruch2 ERMS cells and 20 days for Rh36 cells (10^4 cells plated per well). (W-Y) Quantification of rhabdosphere colony formation (10^4 and 10^3 cells/plated per well, quantification at 10 days for RD and Ruch2 cells and at 20 days for Rh36 cells). Representative experiments showing average colony number of three technical

replicates. Three independent experiments (n=3) for each cell line were performed with a similar effect observed across all biological replicates. ***p<0.001, compared to colony formation in shRNA control cells. Error bars represent standard deviation.

Figure 5. Vangl2 elevates tumor propagating cell number 9-fold in zebrafish *kRASG12D*-induced ERMS. (A-D) Representative images of syngeneic zebrafish engrafted with $1x10^4$ sorted GFP+ ERMS cells and analyzed at 30 days post transplantation. ERMS expressing *rag2*:kRASG12D + *rag2:*GFP (A,B) or *rag2*:kRASG12D + *rag2*:Vangl2 + *rag2:*GFP (C,D). Representative images of tumor histology (B,D). (E) Quantification of fish engrafted with 10^4, 10^3 and 10^2 GFP+ tumor cells that co-expressed *rag2*:kRASG12D with or without *rag2*:Vangl2 (data compiled from engraftment of 3 independent tumors/genotype). (F) Graphical analysis of Extreme Limiting Dilution Analysis (ELDA) denoting overall engraftment rates at various cell dilutions. Dotted lines represent 95% confidence intervals. Estimated tumor propagating cell number for each genotype is noted (data compiled from engraftment of 3 independent unmixed tumors/genotype). ***p<0.001. (G) Quantitative RT-PCR gene expression analysis performed on sorted *rag2*:GFP ERMS cells (independent ERMS are represented and numbered on the x-axis). **p<0.01, ***p<0.001, n.s. not significant, two-way ANOVA. Error bars denote standard deviation.

Figure 6. *vangl2*:mCherry enriches for self-renewing TPCs in zebrafish *kRASG12D*-induced ERMS. (A,B) Transgenic zebrafish with primary ERMS expressing *vangl2(-5kb)*:mCherry and Tg(*myf5*:GFP). (C-E) Transplant fish engrafted with unsorted *myf5*:GFP/*vangl2*:mCherry ERMS shown 30 days post transplantation. Whole animal imaging (C), histology (D), and FACS of ERMS cells obtained at sacrifice (E). (F-J) Syngeneic zebrafish engrafted with purified *myf5*:GFP+/*vangl2*:mCherry+ ERMS cells. Sort purity of

engrafted cells is denoted in the lower left panel of F. Whole animal imaging (F), histology (G), and FACS of ERMS cells obtained at sacrifice (H). (I) Quantification of engraftment of *myf5*:GFP+/*vangl2*:mCherry+ (G+R+, yellow), *myf5*:GFP+/*vangl2*:mCherry- (G+, green) and *myf5*:GFP-/*vangl2*:mCherry+ (R+, red) tumor cells (data is compiled from 4 independent ERMS and shown as individuals in Supplementary Table 3, n=170 recipient fish total). Number of engrafted animals is denoted and percent engraftment annotated by colored bars (+). (J) Graphical analysis of Extreme Limiting Dilution Analysis (ELDA) with the fraction of TPCs found in each sorted cell fraction denoted. Dotted lines represent 95% confidence intervals. ***p<0.001 (data compiled from 4 independent tumors, as above). (K) Quantitative RT-PCR gene expression analysis performed on sorted *myf5*:GFP+/*vangl2*:mCherry+ (G+R+, yellow), *myf5*:GFP+/*vangl2*:mCherry- (G+, green), *myf5*:GFP-/*vangl2*:mCherry+ (R+, red) and *myf5*:GFP-/*vangl2*:mCherry- (NEG, white) cells. Relative expression for each gene is depicted and displayed for each subpopulation. Analysis is representative of two independent tumors (n=2) run as technical triplicates. *myf5*:GFP+/*vangl2*:mCherry+ cells enrich for markers of ERMS TPCs including *c-met, myf5, fgfr1a, and fgfr3* (p<0.01, Student's t-test).

Figure 7. RHOA regulates TPC growth and maintenance downstream of VANGL2 in human RMS. (A) Western blot analysis depicting VANGL2 and RHOA protein in RD cells grown as adherent (2D) cells or in sphere culture for 5 and 10 days. Relative protein expression was normalized to GAPDH. (B) Western blot of total RHOA and activated RHOA (RHOA-GTP) in RD cells stably infected with scramble shRNA (shSCRM) or VANGL2 shRNA (shVL2(1), shVL2(2)) +/- $RHOA^{V14}$ or $RHOA^{N19}$ expression vectors. Relative RHOA/RHOA-GTP protein is indicated for control and VANGL2 knock-down cells. (C) Quantification of RD rhabdosphere colony number at 10 days (10^4 cells plated per well). Representative experiment showing average colony number over three technical replicates. Three

independent experiments (n=3) were performed with a similar effect observed across all biological replicates. (D) Quantitative real-time PCR gene expression analysis of differentiation genes (*MCAD, MYOD, MYOG*) confirming that $RHOA^{V14}$ restores VANGL2-depleted cells to a more undifferentiated state. (E-G) Validation experiments completed using Rh36 ERMS cells. VANGL2 and RHOA protein expression in Rh36 (E) cells grown as adherent (2D) cells or in rhabdosphere culture. Relative protein expression normalized to GAPDH is indicated. (F) Western blot analysis of total RHOA and activated RHOA (RHOA-GTP) in Rh36 cells stably infected with scramble shRNA (shSCRM) or VANGL2 shRNA (shVL2(1), shVL2(2)) +/- $RHOA^{V14}$ or $RHOA^{N19}$ expression vectors. Relative RHOA/RHOA-GTP protein is indicated for control and VANGL2 knock-down cells. (G) Quantification of Rh36 rhabdosphere colony number at 20 days (10^4 cells plated per well). Representative experiment showing average colony number over three technical replicates. Three independent experiments (n=3) were performed with a similar effect observed across all biological replicates. For all graphs *p<0.05, **p<0.01, ***p<0.001, Student's t-test. Error bars represent standard deviation.

STAR Methods

Contact for Reagent and Resource Sharing

Further information and requests for resources and reagents should be directed to and will be fulfilled by the Lead Contact, David M. Langenau, Ph.D. (dlangenau@mgh.harvard.edu).

Experimental Model and Subject Details

Animals

Studies were approved by the Massachusetts General Hospital Subcommittee on Research Animal Care under protocol #2011 N000127 (zebrafish) and #2013 N000038 (mouse). Zebrafish used include: CG1 strain (Mizgireuv and Revskoy, 2006), *mylz2*:mCherry (Xu et al., 1999), and *myf5*:GFP transgenic zebrafish (Chen et al., 2007) bred into the CG1 background for 16-20 generations (Ignatius et al., 2012). Male and female zebrafish were used in all experiments. 8 to 12-week-old *NOD/SCID/Il2rg* null female mice were used for xenograft experiments and were obtained from Jackson laboratory, Bar Harbor, Maine.

Human RMS cell lines

Human RD cells were obtained from ATCC's cell biology collection (Manassas, Virginia). SMS-CTR, 381T, Rh3, Rh5 and Rh30 cell lines were kindly provided by Dr. Corrine Linardic (Duke University, North Carolina), Rh18 cells by Dr. Peter Houghton (Greehey Children's Cancer Research Institute), RMS176 and RMS559 cells by Dr. Jonathan Fletcher (Brigham and Women's Hospital, Massachusetts). Ruch2 and Rh36 cells were kindly provided by Dr. Beat Schäfer (University Children's Hospital, Zurich, Switzerland). Cells were maintained at 37°C in DMEM (Life Technologies) supplemented with 10% FBS (Atlanta Biologicals) and 1% Penicillin/Streptomycin (Life Technologies). Rhabdospheres were

cultured at 37°C in Neurobasal medium supplemented with 20ng/mL EGF, 20ng/mL bFGF, 10ng/mL PGDF-AA, 10ng/mL PDGF-BB, 2x B27 and 1% Penicillin/Streptomyocin. All cells were verified by STR profiling prior to use.

Method Details

Micro-injection and ERMS generation

rag2:kRASG12D and *rag2:GFP* DNA were previously described (Jessen et al., 2001; Langenau et al., 2007). *rag2*:Vangl2 and *vangl2(-5kb)*:mcherry were generated by Gateway cloning using the zebrafish *rag2* or *vangl2(-5kb)* promoter (Jessen et al., 2001; Sittaramane et al., 2013), Vangl2 (gift of Brian Ciruna, Hospital for Sick Children) and mcherry ORF (http://tol2kit.genetics.utah.edu). Plasmid DNA was linearized using NotI and/or XhoI (*rag2:kRASG12D, rag2:GFP*) or HpaI (*vangl2*:mCherry), phenol:chloroform-extracted and re-suspended in 0.5x Tris EDTA + 0.1 M KCl. 2-4pg of linearized DNA was injected into one-cell stage embryos. Tumors were detected using epifluorescence (Olympus MVX10) and GFP-positivity within the body musculature starting at 15 days of life.

Quantification of zebrafish RMS size and initiation

Zebrafish were followed for time to tumor onset using an epifluorescent stereomicroscope. Primary tumor size was quantified at 30 days using GFP fluorescence intensity multiplied by the pixel area using ImageJ software package. Differences in tumor onset were assessed using the method of Kaplan-Meier (Graphpad Prism Software).

Histology and Immunohistochemistry

Zebrafish and xenografted tumors were fixed in 4% PFA, processed and embedded in paraffin Histological sections were made and stained with either Hematoxylin and Eosin or specific antibodies indicated and outlined in the reagents table. The RMS tumor microarray was generously provided by Dr. Matt van de Rijn (Stanford University Medical Centre, TA-23-66). All sectioning and histopathology procedures were performed at the MGH and BWH DF/HCC Research Pathology Cores. VANGL2 (clone 2G4 from Dr. Jean-Paul Borg and subsequently Millipore) was used Pathology review and staging were completed by a board-certified sarcoma pathologist (G.P.N.).

FACS and ERMS cell transplantation

Unsorted primary zebrafish ERMS tumor cells were transplanted at 10^4 cells into 6-10 syngeneic fish. Transplanted tumor cells were allowed to engraft and grow in secondary host animals to expand all tumor cell populations *in vivo*. When secondary recipient animals became moribund, ERMS were harvested in 0.9x PBS supplemented with 5% FBS, stained with DAPI to exclude dead cells and sorted twice using a Laser BD FACSAria II Cell Sorter. Sort purity and viability were assessed after two rounds of sorting and are reported in the context of each experiment. ERMS tumors that were fluorescently labeled with GFP or mCherry were transplanted into syngeneic CG1 zebrafish and monitored for tumor engraftment under a fluorescent dissecting microscope from 10 to 120 days post transplantation. Tumor-propagating cell frequency was quantified following transplantation using the Extreme Limiting Dilution Analysis software package (http://bioinf.wehi.edu.au/software/elda/). ERMS *rag2*:GFP and *myf5*:GFP/*vangl2*:mCherry subpopulations were sorted and RNA extraction was performed using RLT buffer/RNeasy Mini Kit as per manufacturer's instructions. Subsets of tumors were fixed in 4% PFA, sectioned and stained with Hematoxylin and Eosin.

Gene expression analysis

RNA isolation and cDNA preparation were performed as previously described (Chen et al., 2014; Ignatius et al., 2012). Quantitative real-time PCR was completed using a Roche Lightcycler 480. PCR primers are available in Supplemental Table 4 and 5.

Bioinformatic analysis of human RMS samples

RNA sequencing data was processed and analyzed as previously reported (Shern et al., 2014, GEO Accession # GSE108022). RNAseq reads were aligned to the human reference genome (hg19) using TopHat to generate BAM files. Gene expression was calculated as Fragments Per Kilobase of transcript per Million mapped reads (FPKM) using Cufflinks and with UCSC reference and reported at the gene level. Sample groups were determined based on genetic presence or absence of the fusion gene, as previously reported (Shern et al., 2014). Data visualization and statistical Student's t-test were performed using FPKM values of *VANGL2* using Graphpad Prism software. The 12 primary patient samples analyzed by quantitative RT-PCR in Figure 1C have been reported previously (Ignatius et al., 2017).

Protein extraction, Immunoprecipitation, Immunofluorescence and Western blot analysis

Total cellular protein from human RMS cell lines was obtained by lysis in 2% SDS buffer supplemented with protease inhibitors (Santa Cruz Biotechnology). Samples were boiled, vortexed and homogenized by passage through a syringe. 20-50ug of protein was loaded onto 4-20% Mini-Protean TGX gels (Biorad) and transferred onto PVDF membranes. GTP-bound RHOA and RAC1 were precipitated using pull-down activation assay Biochem Kits, according to manufacturer's recommendations (Cytoskeleton). Antibodies against

VANGL2 (2G4, Dr. Jean-Paul Borg and Millipore), PAX7 (DSHB), MYOG (Santa Cruz, M-225), FGFR3 (Cell Signaling, C51F2), CD133 (Cell Signaling, D2V8Q), GAPDH (Cell Signaling, 14C10), RHOA (Cell Signaling, 67B9), RAC1 (Cytoskeleton, C7H2) were used. Uninfected or stably-infected cells were plated in flat, clear bottom 96 well plates and fixed at the specified time point in 4% PFA/PBS for 15 minutes at room temperature. Cells were washed in 1x PBS, permeabilized in 0.5% TritonX-100/PBS, washed in 0.1% PBST and incubated with primary antibody overnight. Fluorescently-conjugated secondary antibody was used at 1:1000 dilution with 1:5000 DAPI to stain nuclei. Cells were washed in 1x PBS and imaged using a LSM710 Zeiss Laser scanning confocal microscope. Images were processed using ZEN software and and quantifications were made using ImageJ software.

Plasmids, lentiviral and shRNA

Lentiviral work was approved by Partners IBC under protocol #2013B000039. shRNA plasmids in the pLKO.1- background vector targeting VANGL2 (shVL2(1) – CAAGTCACACAAGTTTGTCAT, shVL2(2) – TTCAAACTCTCCGAGGAATTT) were obtained from the Massachusetts General Hospital Molecular Profiling Core Facility. RHOAV14, RHOAN19, RAC1V12, and RAC1N17 over-expression vectors were generated using a primer based mutagenesis approach and cloning from wild-type RHOA and RAC1 transcript. Clones were inserted into pDONR221 and pLentiCMVPuroDEST (w118-1) vectors using standard Gateway cloning approaches.

All vectors were packaged using 293T cells. 2µg pCMV-dR8.91 and 0.2µg pVSV-g were transfected with Trans-LTI reagent (Life Technologies) according to manufacturer's recommendation. RMS were infected with 1:1 volume viral particle to DMEM/10%FBS media containing 1:1000 Polybrene (EMD Millipore) for 24 hours. Cells were maintained in DMEM/10% FBS media and selected for stable infection with puromycin after 48 hours.

Mouse xenograft, bioluminescent imaging, and necropsy

RD ERMS, SMSCTR ERMS and RH30 ERMS cells were co-infected with pLKO.1-shRNA and pLKO.1-*luc-mKate* (gift of Drs. Matthijssens and Van Vlierberghe, Ghent University, Belgium). At 3 days post-infection without selection, cells were collected, counted and analyzed using the SORP4 Laser BD LSRII Flow Cytometer to determine viability using DAPI and mKate expression, to infer infection efficiency. Equal numbers of viable cells were embedded into matrigel at $1x10^6$ cells/100uL. 8 to 12-week-old NOD/SCID/IL2g-null female mice were anesthetized using isofluorane and injected with shSCRM/luc-mKate cells subcutaneously into the left flank and shVANGL2/luc-mKATE cells into the right flank (200uL/flank injection, n=6 animals/shRNA construct). Tumor growth was monitored weekly by bioluminescence imaging following subcutaneous injection of 75mg/kg D-luciferin (Perkin Elmer) in 100uL PBS. Imaging was performed and analyzed using the IVIS Lumina II (Caliper Life Science). At necropsy, tumor volume was calculated using a caliper measure and tumor mass was determined using a standard weight scale.

Quantification and Statistical Analysis

Statistical details for all experiments can be found in the Results section and Figure legends. Data in bar graphs is shown as an absolute number or mean ± SD (standard deviation), as indicated. Student's t-tests were used to calculate significant differences between normally distributed data, where indicated. Grouped data was analyzed using two-way ANOVA. Extreme Limiting Dilution Analysis (ELDA, http://bioinf.wehi.edu.au/software/elda/) was used to analyze results of limiting dilution experiments. P-values less than 0.05 were considered to be statistically significant. Significance is indicated as asterisk and defined in the Figure legends. Zebrafish and mice were randomly assigned to experimental groups.

Data and Software Availability

The data set described in Shern et al. 2014 was analyzed as described in the Results section and is deposited in GEO, Accession Number GSE108022.

Key Resources Table

REAGENT or RESOURCE	SOURCE	IDENTIFIER
Antibodies		
Rat monoclonal anti-VANGL2	Millipore	Cat. #MABN750, AB_2721170
Mouse monoclonal anti-Pax7	DSHB	Cat. #Pax7, AB_528428
Rabbit polyclonal anti-Myogenin	Santa Cruz	sc-576, AB_2148908
Rabbit monoclonal anti-FGFR3	Cell Signaling	Cat. #4574, AB_2721171
Rabbit monoclonal anti-CD133	Cell Signaling	Cat. #64326, AB_27211172
Rabbit monoclonal anti-GAPDH	Cell Signaling	Cat. #2118, AB_561053
Rabbit monoclonal anti-RhoA	Cell Signaling	Cat. #2117, AB_10693922
Mouse monoclonal anti-Rac1	Cytoskeleton	Cat. #ARC03, AB_2721173
Rabbit monoclonal anti-Ki67	Abcam	Cat. #ab16667, AB_302459
Rabbit monoclonal anti-Ki67	Biocare	Cat. #CRM325, AB_2721189
Rabbit monoclonal anti-CC3 (Asp175)	Cell Signaling	Cat. #9664, AB_2070042
Mouse monoclonal anti-MYOD	Dako	Cat. #M2512, AB_2721191
Mouse monoclonal anti-MYOG	Dako	Cat. #M3559, AB_2250893
Rabbit polyclonal anti-RFP	Abcam	Cat. #152123, AB_2637080
Anti-Rabbit IgG, HRP-linked	Cell Signaling	Cat. #7074, AB_2099233
Anti-Rat IgG, HRP-linked	Thermo Fisher	Cat. # PA128573, AB_10980086
Anti-goat IgG, Alexa Fluor 488	Life Technologies	Cat. #A11055, AB_2534102
Anti-mouse IgG, Alexa Fluor 594	Life Technologies	Cat. #A11062, AB_2534109
Anti-rabbit IgG, Alexa Fluor 594	Life Technologies	Cat. #A21207, AB_141637
Chemicals, Peptides, and Recombinant Proteins		

EGF	Life Technologies	Cat. #PHG0311
bFGF	Life Technologies	Cat. #13256029
PGDF-AA	Life Technologies	Cat. #PHG0035
PGDF-BB	Life Technologies	Cat. #PHG0045
B27 (50x)	Life Technologies	Cat. #17504044
Neurobasal Medium	Life Technologies	Cat. #21103049
DMEM	Life Technologies	Cat. #11995073
Opti-MEM Reduced Serum Medium	Life Technologies	Cat. #31985088
Transit LT-1	VWR	Cat. #MIR2300
Polybrene Infection Reagent	Millipore	Cat. #TR-1003-G
Puromycin	Fisher Scientific	Cat. #NC9138068
Penicillin-Streptomycin-Glutamine	Life Technologies	Cat. #10378-016
Fetal Bovine Serum	Atlanta Biologicals	Cat. #S11550H
Trypsin/EDTA Solution (TE)	Life Technologies	Cat. #R001100
PBS	Life Technologies	Cat. #10010049
DAPI	Life Technologies	Cat. #D1306
Not1	New England Biolabs	Cat. #R3189
XhoI	New England Biolabs	Cat. #R0146
HpaI	New England Biolabs	Cat. #R0105
PVDF Transfer Membranes	Bio-Rad Laboratories	Cat. #1704157
Mini-Protean TGX Gels	Bio-Rad Laboratories	Cat. #456-1094
ECL Prime Western Blot Detection Reagent	Fisher Scientific	Cat. #45002401
Gateway BP Clonase II	Life Technologies	Cat. #11789020
Gateway LR Clonase II Plus	Life Technologies	Cat. #11791020
Light Cycler 480 SYBR Green	Roche	Cat. #04887352001
Matrigel	VWR	Cat. #47743-715
D-Luciferin	Perkin Elmer	Cat. #122799
Critical Commercial Assays		
RhoA Pull-down Activation Assay Biochem Kit	Cytoskeleton	Cat. #BK036
Rac1 Pull-down Activation Assay Biochem Kit	Cytoskeleton	Cat. #BK035
RNeasy Mini Kit	Qiagen	Cat. #74106
cDNA Reverse Transcription Kit	Life Technologies	Cat. #4368813
Click-IT EDU Kit	Life Technologies	Cat. #C10269
Deposited Data		
RNA sequencing of human RMS	Shern et al. 2014	GEO Accession # GSE108022
Experimental Models: Cell Lines		
HEK293T	ATCC	CRL-3216
RD	ATCC	CCL-136
SMSCTR	Corrine Linardic (Duke University)	n/a
381T	Corrine Linardic (Duke University)	n/a
Rh3	Corrine Linardic (Duke University)	n/a
Rh5	Corrine Linardic (Duke University)	n/a
Rh30	Corrine Linardic (Duke University)	n/a

Rh18	Peter Houghton (Greehey Children's Cancer Research Institute)	n/a
RMS176	Johnathan Fletcher (Brigham and Women's Hospital)	n/a
RMS559	Johnathan Fletcher (Brigham and Women's Hospital)	n/a
Ruch2	Beat Schäfer (University Children's Hospital, Zurich)	n/a
Rh36	Beat Schäfer (University Children's Hospital, Zurich)	n/a
Experimental Models: Organisms/Strains		
Zebrafish CG1 strain	Mizgireuv and Revskoy, 2006	n/a
Zebrafish Tg(*mylz2*:mCherry)	Xu et al. 1999, Ignatius et al. 2012	n/a
Zebrafish Tg(*myf5*:mCherry)	Chen et al. 2007, Ignatius et al. 2012	n/a
Mice *NOD/SCID/Il2rg*-null	Jackson laboratories	Cat. #005557
Oligonucleotides		
Primers for qRT-PCR related to human RMS	Table S4	n/a
Primers for qRT-PCR related to zebrafish ERMS	Table S5	n/a
Recombinant DNA		
rag2:KRAS^{G12D}	Langenau et al. 2007	n/a
rag2:GFP	Jessen et al. 2001	n/a
rag2:Vangl2	This paper with *rag2* from Jessen et al. 2001	n/a
vangl2(-5kb):mCherry	This paper with p5E *vangl2(-5kb)* (gift of Anand Chandrasekhar, Sittaramane et al. 2013)	n/a
pME-Vangl2	Gift of Brian Ciruna (Hospital for Sick Children, Toronto)	n/a
pDONR221	Koichi Kawakami, Kristen Kwan	http://tol2kit.genetics.utah.edu
pDESTTol2pA2	Koichi Kawakami, Kristen Kwan	http://tol2kit.genetics.utah.edu
pME-mCherry	Koichi Kawakami, Kristen Kwan	http://tol2kit.genetics.utah.edu
psPAX2	Addgene	Plasmid #12260
pVSV-g	Addgene	Plasmid #8454
pLKO scramble shRNA	Addgene	Plasmid #1864

pLKO.1 shVANGL2(1)	Massachusetts General Hospital Molecular Profiling Facility	TRCN0000147138
pLKO.1 shVANGL2(2)	Massachusetts General Hospital Molecular Profiling Facility	TRCN0000417141
pLKO.1-luc-mKate	gift of Drs Van Vlierberghe and Matthijssens (Ghent University)	n/a
pLentiCMVPuroDEST	Addgene	w118-1
pLentiCMV-RHOA^{V14}	This reagent was created from PCR of endogenous human RHOA and the point mutation generated by modifying the specific oligonucleotide primer. RHOA^{V14} was cloned into pLentiCMVPuroDEST using standard gateway approach	
pLentiCMV-RHOA^{N19}	This reagent was created from PCR of endogenous human RHOA and the point mutation generated by modifying the specific oligonucleotide primer. RHOA^{N19} was cloned into pLentiCMVPuroDEST using standard gateway approach	
pLentiCMV-RAC1^{V12}	This reagent was created from PCR of endogenous human RAC1 and the point mutation generated by modifying the specific oligonucleotide primer. RAC1^{V12} was cloned into pLentiCMVPuroDEST using standard gateway approach	

pLentiCMV-RAC1^{N17}	This reagent was created from PCR of endogenous human RAC1 and the point mutation generated by modifying the specific oligonucleotide primer. RAC1^{N17} was cloned into pLentiCMVPuroDEST using standard gateway approach	
Software and Algorithms		
GraphPad Prism	GraphPad	https://www.graphpad.com/scientific-software/prism/
ImageJ	National Institutes of Health	https://imagej-nih-gov.ezp-prod1.hul.harvard.edu/ij/
ZEN	Carl Zeiss	https://www.zeiss.com/microscopy/int/products/microscope-software/zen.html
Extreme Limiting Dilution Analysis (ELDA)	Walter & Eliza Hall Institute of Medical Research	http://bioinf.wehi.edu.au/software/elda/
IVIS Lumina II Living Image	Perkin Elmer	Part # 28110
Other		
Pediatric sarcoma tissue microarray	Matt va de Rijn (Stanford University Medical Cener)	TA-23-66
Primary human RMS RNA/cDNA (12 samples + cell lines)	David Malkin (Hospital for Sick Children, Toronto), described previously in Ignatius et al. 2017	n/a

Figure 1.

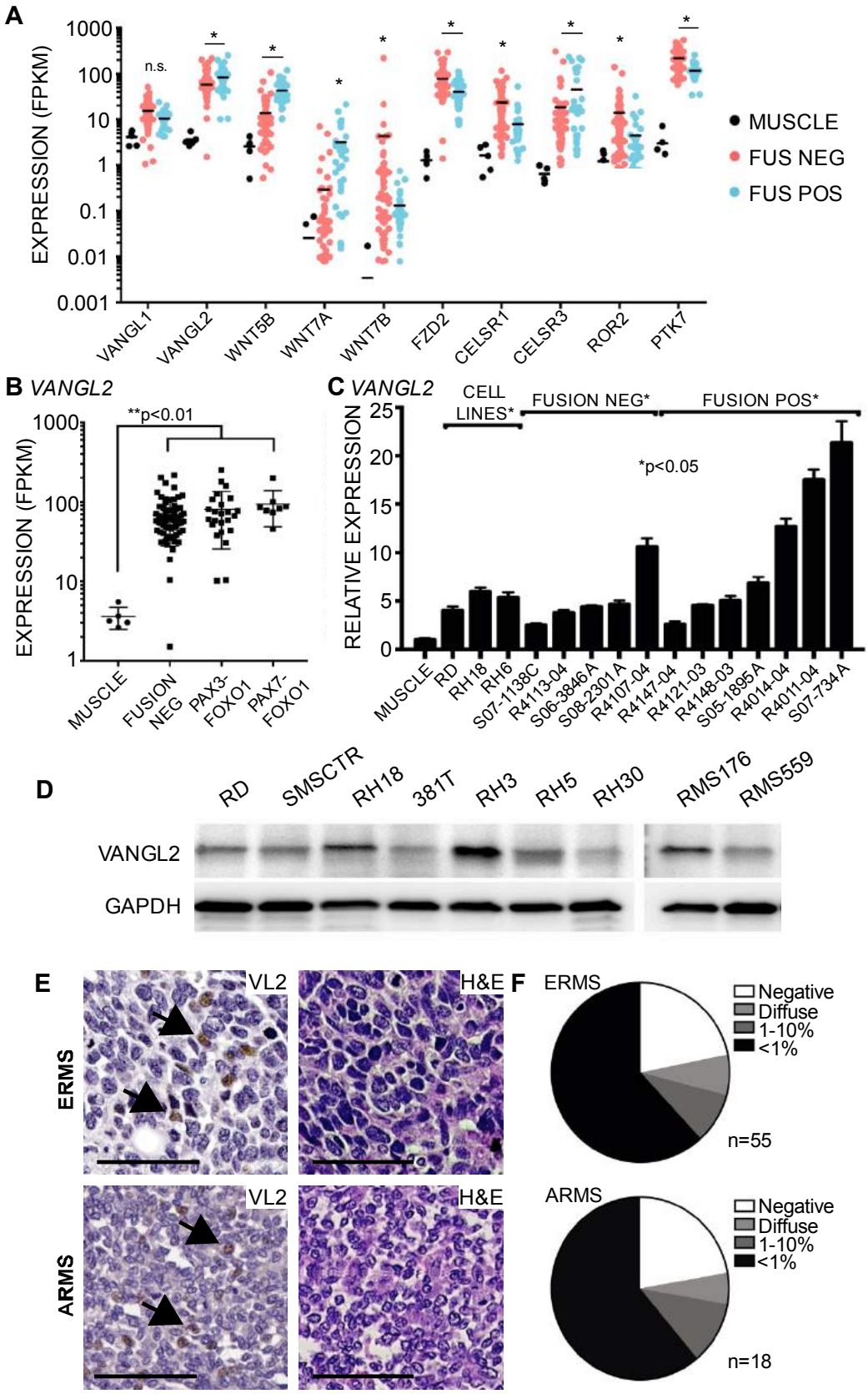
A
EXPRESSION (FPKM)
1000
100
10
1
0.1
0.01
0.001
n.s.
*
VANGL1
VANGL2
WNT5B
WNT7A
WNT7B
FZD2
CELSR1
CELSR3
ROR2
PTK7
MUSCLE
FUS NEG
FUS POS
B VANGL2
**p<0.01
EXPRESSION (FPKM)
MUSCLE
FUSION NEG
PAX3-FOXO1
PAX7-FOXO1
C VANGL2
CELL LINES*
FUSION NEG*
FUSION POS*
*p<0.05
RELATIVE EXPRESSION
MUSCLE
RD
RH18
RH6
S07-1138C
R4113-04
S06-3846A
S08-2301A
R4107-04
R4147-04
R4121-03
R4148-03
S05-1895A
R4014-04
R4011-04
S07-734A
D
RD
SMSCTR
RH18
381T
RH3
RH5
RH30
RMS176
RMS559
VANGL2
GAPDH
E
ERMS
ARMS
VL2
H&E
F
ERMS
ARMS
Negative
Diffuse
1-10%
<1%
n=55
n=18

Figure 2.

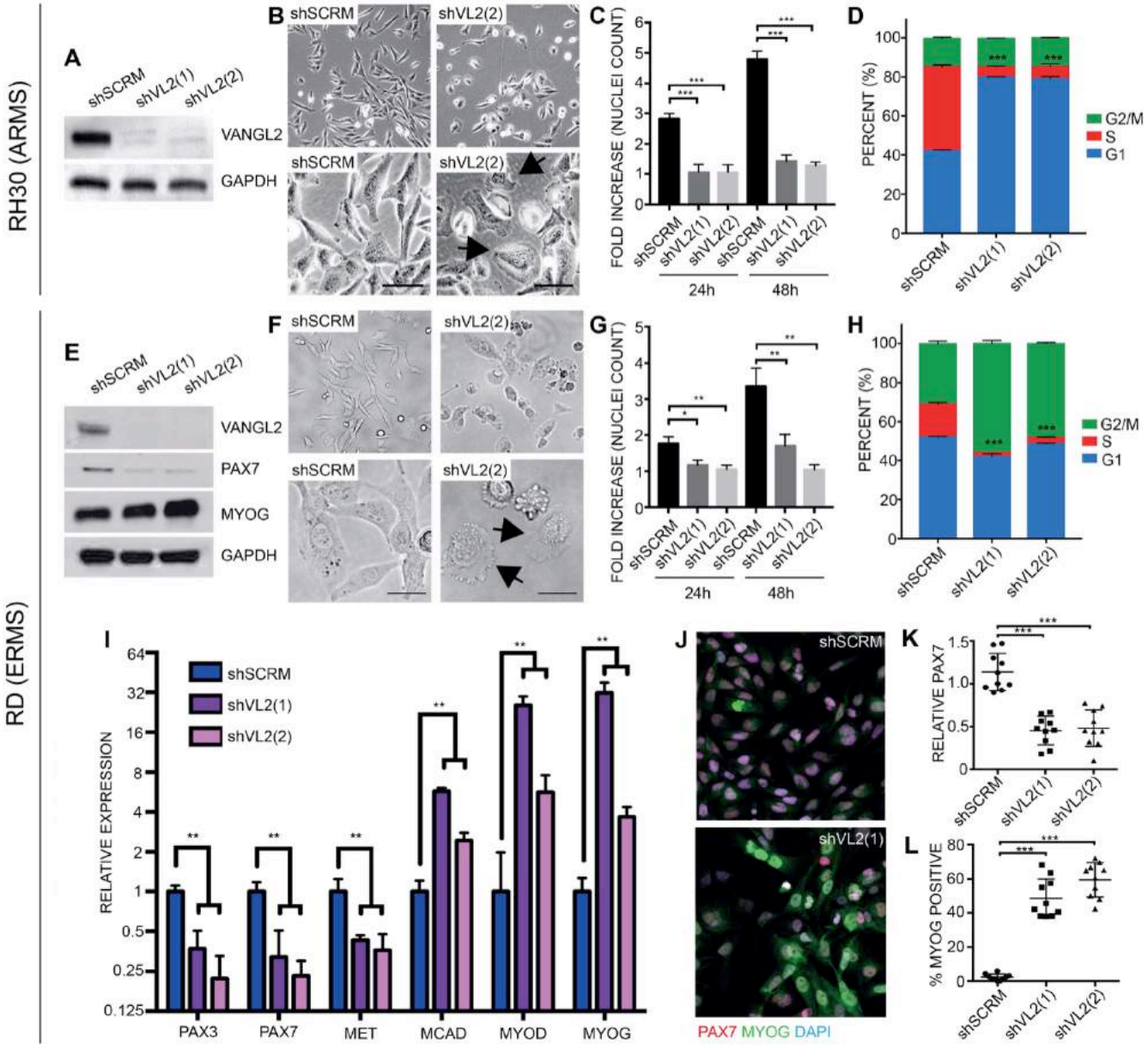
RH30 (ARMS)
RD (ERMS)
A
shSCRM
shVL2(1)
shVL2(2)
VANGL2
GAPDH
B
shSCRM
shVL2(2)
C
FOLD INCREASE (NUCLEI COUNT)
24h
48h
D
PERCENT (%)
G2/M
S
G1
E
PAX7
MYOG
F
G
H
I
RELATIVE EXPRESSION
PAX3
PAX7
MET
MCAD
MYOD
MYOG
J
PAX7 MYOG DAPI
K
RELATIVE PAX7
L
% MYOG POSITIVE

Figure 3.

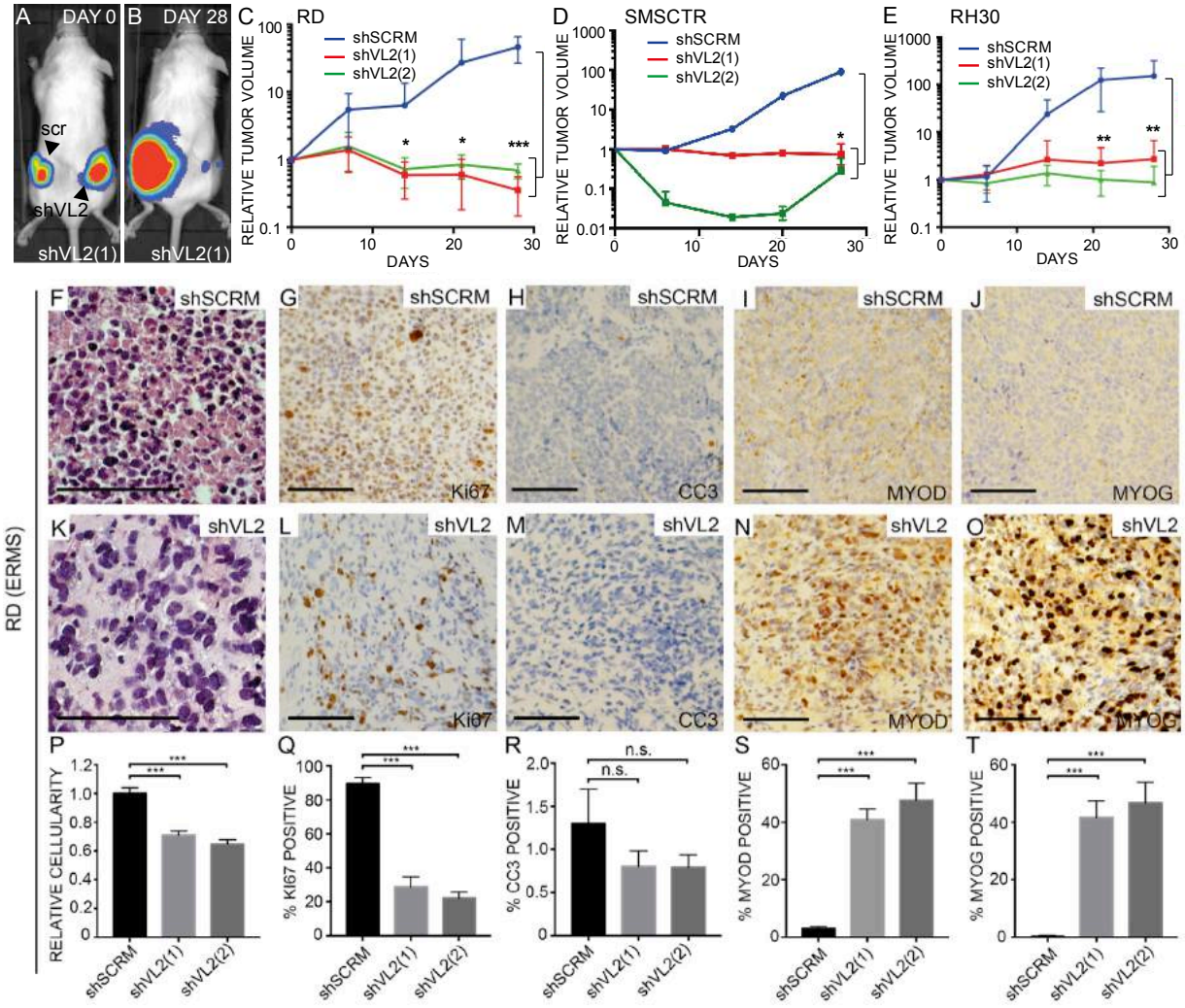
A
DAY 0
B
DAY 28
scr
shVL2
shVL2(1)
shVL2(1)
C
RD
D
SMSCTR
E
RH30
shSCRM
shVL2(1)
shVL2(2)
RELATIVE TUMOR VOLUME
DAYS
RD (ERMS)
F
shSCRM
G
shSCRM
Ki67
H
shSCRM
CC3
I
shSCRM
MYOD
J
shSCRM
MYOG
K
shVL2
L
shVL2
Ki67
M
shVL2
CC3
N
shVL2
MYOD
O
shVL2
MYOG
P
RELATIVE CELLULARITY
Q
% KI67 POSITIVE
R
% CC3 POSITIVE
n.s.
S
% MYOD POSITIVE
T
% MYOG POSITIVE
shSCRM
shVL2(1)
shVL2(2)

Figure 4.

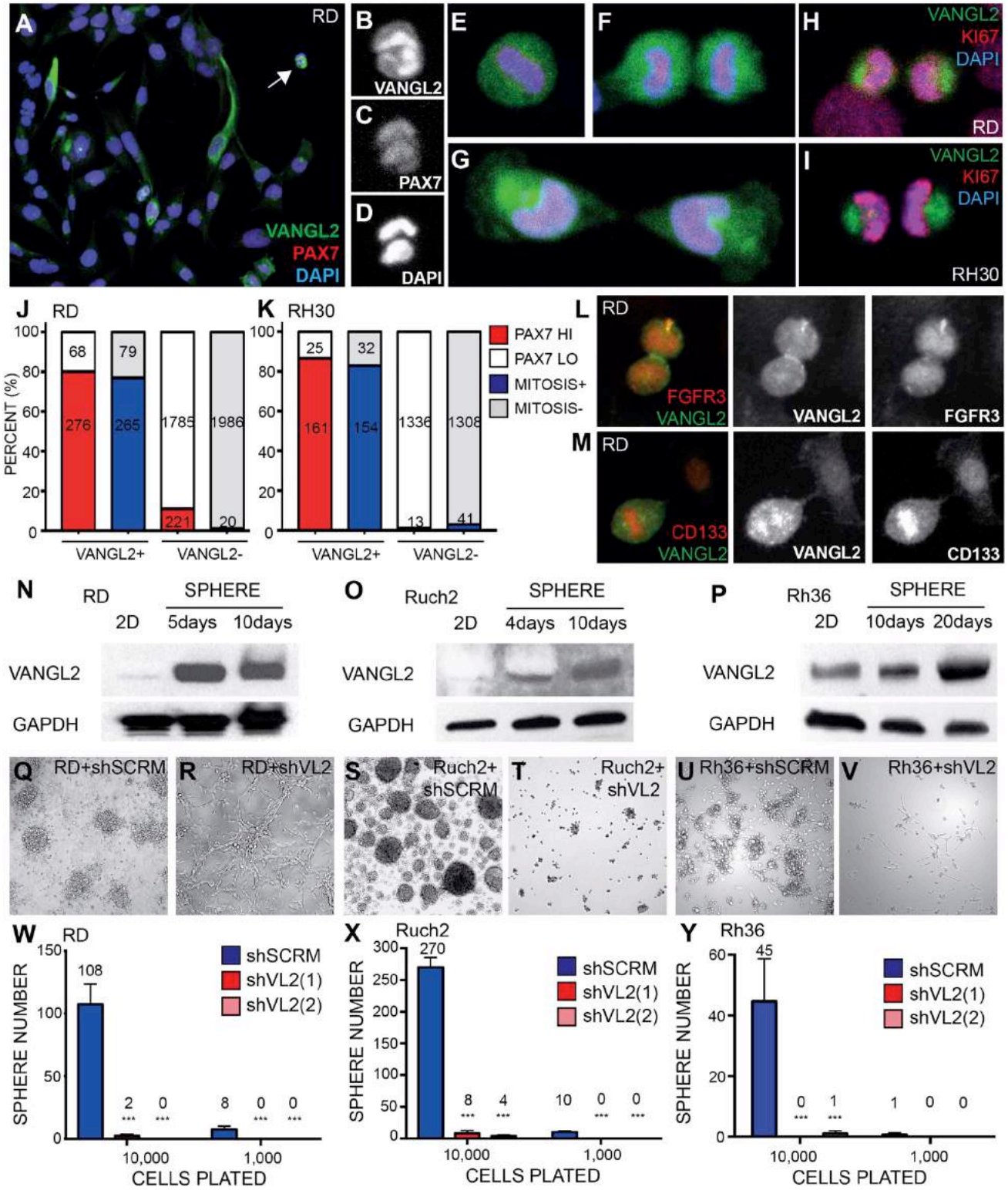
A
RD
VANGL2
PAX7
DAPI
B
VANGL2
C
PAX7
D
DAPI
E
F
G
H
VANGL2
KI67
DAPI
RD
I
VANGL2
KI67
DAPI
RH30
J
RD
K
RH30
PERCENT (%)
PAX7 HI
PAX7 LO
MITOSIS+
MITOSIS-
68
79
276
265
1785
1986
221
20
25
32
161
154
1336
1308
13
41
VANGL2+
VANGL2-
L
RD
FGFR3
VANGL2
VANGL2
FGFR3
M
RD
CD133
VANGL2
VANGL2
CD133
N
RD
SPHERE
2D
5days
10days
VANGL2
GAPDH
O
Ruch2
SPHERE
2D
4days
10days
VANGL2
GAPDH
P
Rh36
SPHERE
2D
10days
20days
VANGL2
GAPDH
Q
RD+shSCRM
R
RD+shVL2
S
Ruch2+
shSCRM
T
Ruch2+
shVL2
U
Rh36+shSCRM
V
Rh36+shVL2
W
RD
X
Ruch2
Y
Rh36
SPHERE NUMBER
shSCRM
shVL2(1)
shVL2(2)
108
2
0
8
0
0
270
8
4
10
0
0
45
0
1
1
0
0
10,000
1,000
CELLS PLATED

Figure 5.

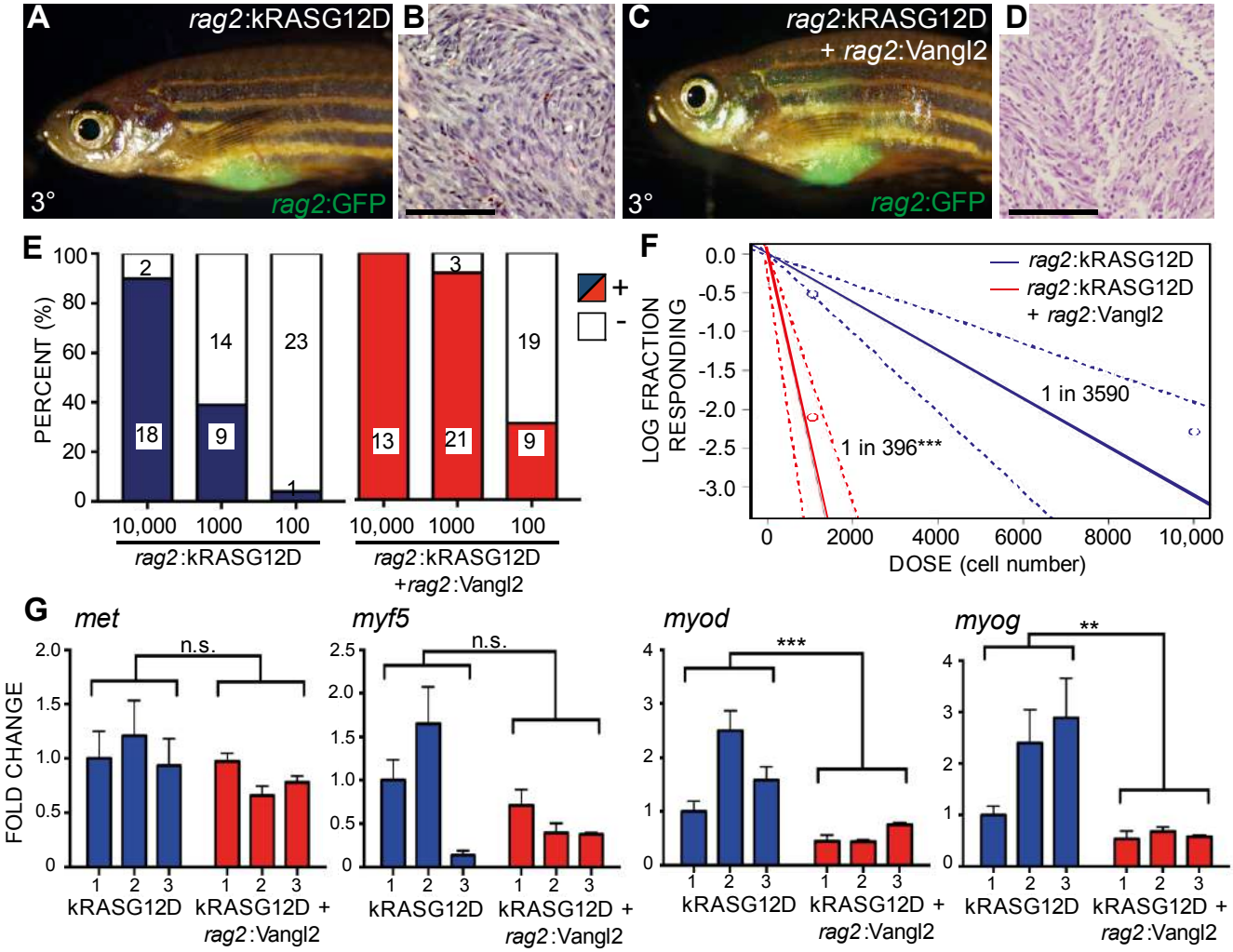
A
rag2:kRASG12D
3°
rag2:GFP
B
C
rag2:kRASG12D
+ rag2:Vangl2
3°
rag2:GFP
D
E
PERCENT (%)
100
80
60
40
20
0
2
18
14
9
23
1
3
13
21
19
9
+
-
10,000 1000 100
rag2:kRASG12D
10,000 1000 100
rag2:kRASG12D
+rag2:Vangl2
F
LOG FRACTION RESPONDING
0.0
-0.5
-1.0
-1.5
-2.0
-2.5
-3.0
rag2:kRASG12D
rag2:kRASG12D
+ rag2:Vangl2
1 in 3590
1 in 396***
0
2000
4000
6000
8000
10,000
DOSE (cell number)
G
met
myf5
myod
myog
FOLD CHANGE
n.s.
n.s.
***
**
kRASG12D
kRASG12D +
rag2:Vangl2

Figure 6.

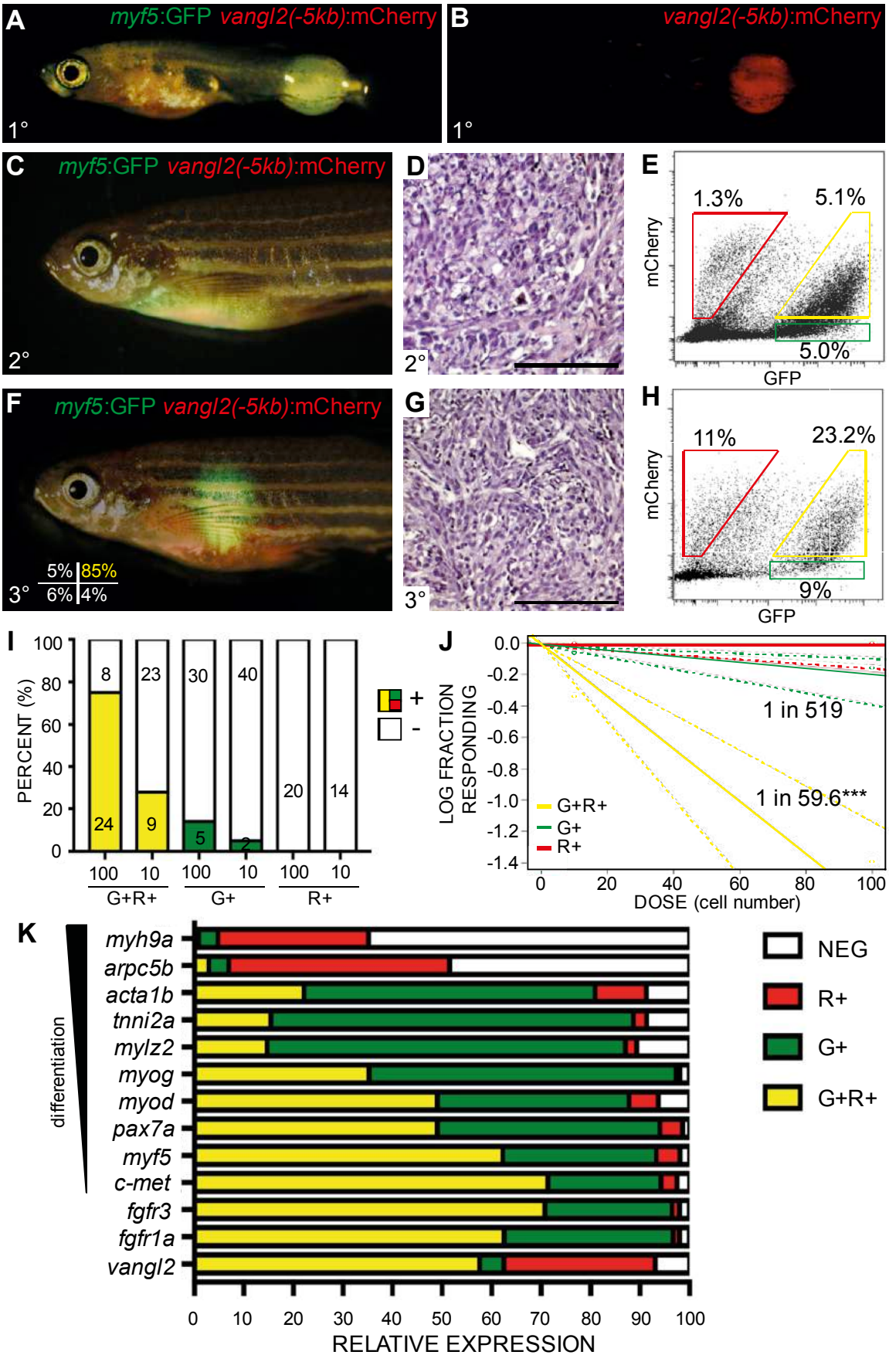
A
myf5:GFP vangl2(-5kb):mCherry
1°
B
vangl2(-5kb):mCherry
1°
C
myf5:GFP vangl2(-5kb):mCherry
2°
D
2°
E
1.3%
5.1%
5.0%
mCherry
GFP
F
myf5:GFP vangl2(-5kb):mCherry
5%
85%
6%
4%
3°
G
3°
H
11%
23.2%
9%
mCherry
GFP
I
PERCENT (%)
100
80
60
40
20
0
8
23
30
40
20
14
24
9
5
2
100
10
100
10
100
10
G+R+
G+
R+
+
-
J
LOG FRACTION RESPONDING
0.0
-0.2
-0.4
-0.6
-0.8
-1.0
-1.2
-1.4
1 in 519
1 in 59.6***
G+R+
G+
R+
0
20
40
60
80
100
DOSE (cell number)
K
differentiation
myh9a
arpc5b
acta1b
tnni2a
mylz2
myog
myod
pax7a
myf5
c-met
fgfr3
fgfr1a
vangl2
0
10
20
30
40
50
60
70
80
90
100
RELATIVE EXPRESSION
NEG
R+
G+
G+R+

Figure 7.

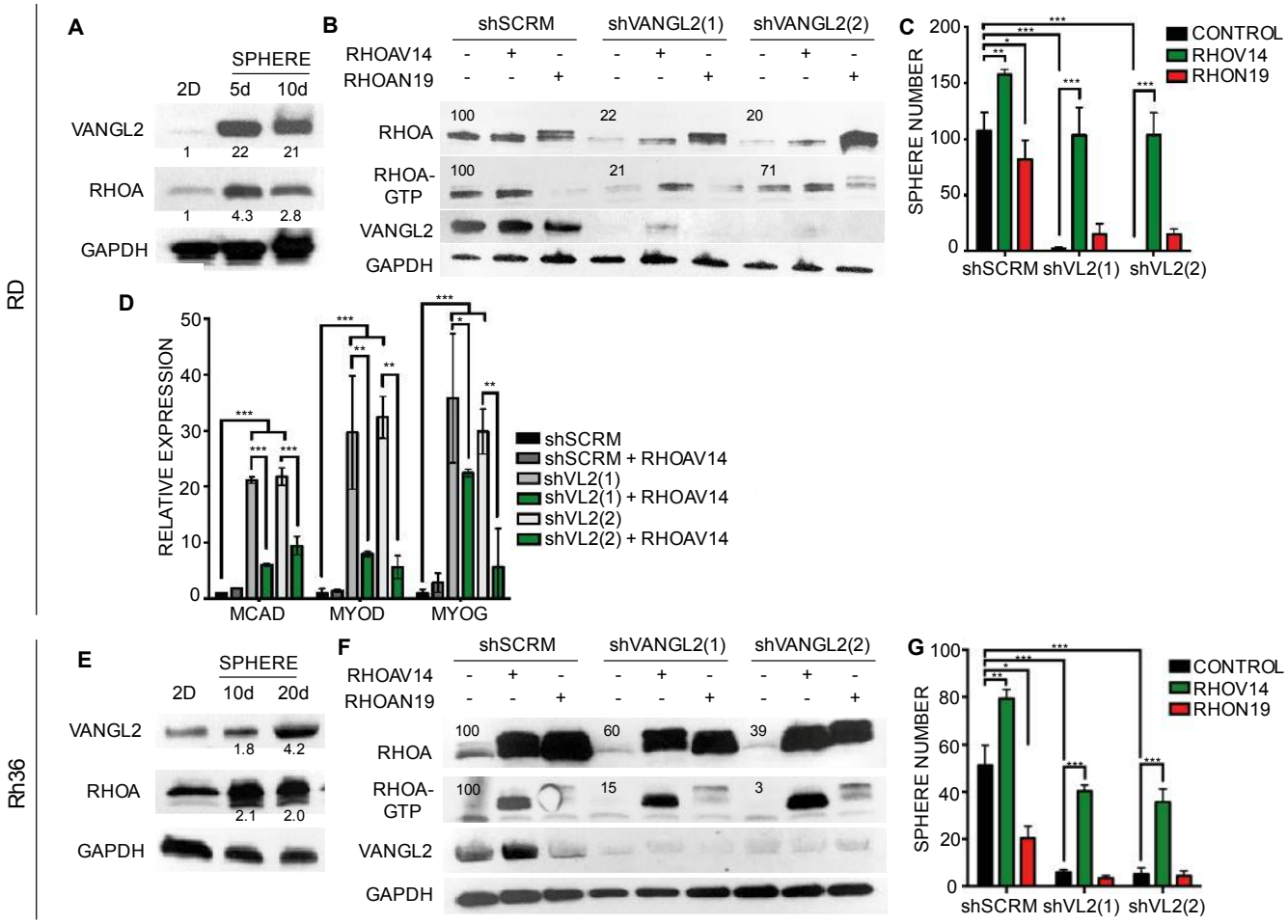
RD
A
SPHERE
2D
5d
10d
VANGL2
1
22
21
RHOA
1
4.3
2.8
GAPDH
B
shSCRM
shVANGL2(1)
shVANGL2(2)
RHOAV14
RHOAN19
RHOA
RHOA-GTP
VANGL2
GAPDH
100
22
20
100
21
71
C
SPHERE NUMBER
CONTROL
RHOV14
RHON19
shSCRM
shVL2(1)
shVL2(2)
D
RELATIVE EXPRESSION
shSCRM
shSCRM + RHOAV14
shVL2(1)
shVL2(1) + RHOAV14
shVL2(2)
shVL2(2) + RHOAV14
MCAD
MYOD
MYOG
Rh36
E
SPHERE
2D
10d
20d
VANGL2
1.8
4.2
RHOA
2.1
2.0
GAPDH
F
shSCRM
shVANGL2(1)
shVANGL2(2)
RHOAV14
RHOAN19
RHOA
RHOA-GTP
VANGL2
GAPDH
100
60
39
100
15
3
G
SPHERE NUMBER
CONTROL
RHOV14
RHON19
shSCRM
shVL2(1)
shVL2(2)

Vangl2/RhoA signaling regulates stem cell self-renewal programs and growth in Rhabdomyosarcoma

Supplemental Information

Supplemental Figure Legends

Figure S1. ***Related to Figure 1.*** **Immunohistochemistry for VANGL2 on primary human sarcoma sections.** (A,B) Representative images of VANGL2 immunohistochemistry performed on primary human ERMS (A) and ARMS (B). Protein expression was quantified based on the percentage of tumor cells that expressed VANGL2. (C) VANGL2 IHC staining in primary Wilm's tumor, Synovial sarcoma and Desmoplastic small round cell tumor (DSRCT). Arrowheads and inserts highlight VANGL2+ cells. Scale bar is 100μm.

Figure S2. ***Related to Figure 3.*** **VANGL2 regulates human xenograft growth and suppresses differentiation in rhabdomyosarcoma.** Xenograft studies for RD ERMS (A-E), SMSCTR ERMS (F-R), and Rh30 ARMS (T-Z). (A,F,T) Western blot analysis following scramble shRNA (shSCRM) and VANGL2 shRNA (shVL2(1), shVANGL2(2)) knockdown in cells prior to xenograft transplantation. Knockdown was performed in two successive experiments in SMSCTR cells and thus, represented independently. GAPDH is used as a loading control. (B,G,U) Luciferase bioluminescent imaging of mice engrafted with scramble shRNA (left, scr) or VANGL2 shRNAs (right, shVL2). Representative animals are shown immediately after injection (0 days) and 28 days post injection. (C,I,V) Bright-field image of whole animal and excised tumors at the time of sacrifice, 38-60 days post transplantation. Only 6 of 12 shVANGL2-infected RD tumors and 5 of 12 shVANGL2-infected SMSCTR

tumors were recovered at necropsy. (D,J,W) Tumor mass and (E,K,X) volume at necropsy. (H) Quantification of tumor size based on bioluminescence relative to day 0 for SMSCTR xenograft experiments. Experiments were completed on different days and hence, control shSCRM results are represented independently here to provide a full assessment of knockdown effects on tumor growth. n=6 animals/arm. (L-O) Representative images of SMSCTR tumors recovered at necropsy and assessed by hematoxylin and eosin staining (L), IHC for Ki67 (M), cleaved caspase 3 (CC3, N), and MYOG (O). (P) Quantification of nuclei counts/tumor area. (Q) Percentage of Ki67 positive cells within tumors. (R) Percentage of cells that stained for activated caspase 3 (CC3). (S) Quantification of immunohistochemical analysis for MYOG. SMSCTR xenografts infected with shVANGL2(1) were not recovered at necropsy and could not be stained (represented as n/a in P-S). (Y,Z) Representative histology of Rh30 tumors at necropsy. H&E staining (Y) and immunohistochemistry for VANGL2 and mKate (Z). mKate IHC was used to detect lentiviral vector pLKO.1-*luc-mKate* and shows that late tumor emergence resulted from engraftment of rare, uninfected Rh30 cells. *, p=0.05; **, p<0.01; ***, p<0.001 by Student's t-test comparison to control animals.

Figure S3. ***Related to Figure 4.*** **VANGL2 is co-expressed with high CD133 and FGFR3 in human RMS cells.** Immunofluorescent staining of VANGL2, CD133 and FGFR3 in RD ERMS (A) and Rh30 ARMS cells (B). VANGL2 (green) is co-expressed with stem cell markers CD133 and FGFR3 (red) in a subset of cells (white arrows). Merged and single fluorescent channels are shown. DAPI was used to stain nuclei. (C,D) Quantification showing the percentage of cells expressing CD133 (red) and FGFR3 (orange) in VANGL2-high versus VANGL2-low expressing RD (C) and Rh30 cells (D).

Figure S4. *Related to Figure 5*. Transgenic expression of *vangl2* does not affect tumor latency, incidence, or size in the primary zebrafish ERMS. (A-D) Zebrafish ERMS generated by injection of *rag2:kRASG12D* (A,B) or *rag2:kRASG12D* + *rag2:vangl2* (C,D). *rag2:GFP* was co-injected to fluorescently label tumor cells. Representative images of tumor histology (B,D). (E) Tumor incidence assessed over time (n=175 animals for kRASG12D and n=214 animals for kRASG12D+Vangl2, p=0.57 log-rank statistic). (F) Tumor size measured at 30 days based on GFP intensity multiplied by 2D pixel area. Each datum point represents tumor size in a single fish. Not significant by Student's t-test calculation (n.s.).

Figure S5. *Related to Figure 6. Vangl2* transcripts are highly expressed in zebrafish TPCs, sort purity for experiments shown in Figure 6 and establishing long-term self-renewal potential of *myf5*:GFP+/*vangl2*:mCherry+ TPCs. (A) Animal shown following engraftment of bulk *myf5*:GFP/*mylz2*:mCherry tumor cells. (B) FACS plot of isolated *myf5*:GFP+/*mylz2*:mCherry- (green), *myf5*:GFP+/*mylz2*:mCherry+ (yellow), *myf5*:GFP-/*mylz2*:mCherry+ (red) and *myf5*:GFP-/*mylz2*:mCherry- (black) ERMS cells. Percentage of cells in each gated sub-population are noted. (C) Quantitative RT-PCR analysis for *vangl2* expression in sorted *myf5*:GFP+/*mylz2*:mCherry- (+/-, green), *myf5*:GFP+/*mylz2*:mCherry+ (+/+, yellow), *myf5*:GFP-/*mylz2*:mCherry+ (-/+, red) and *myf5*:GFP-/*mylz2*:mCherry- (-/-, grey) cells. Sort purity was >85% and >95% cell viability. ***p<0.001, Student's t-test. Error bars represent standard deviation. Graph is representative of n=2 independent ERMS. (D) FACS plots showing sort purity for tumor cells engrafted into recipient animals depicted in Figure 6F-J. (E-H) Establishing long-term self-renewal potential of *myf5*:GFP+/*vangl2*:mCherry+ TPCs. Sort purity of cells isolated from fish engrafted with *myf5*:GFP+/*vangl2*:mCherry+ TPCs (E) and then engrafted into recipient fish F-H. Whole animal fluorescent image (F), histology (G), and quantification of engraftment at varying cell doses (H). *myf5*:GFP+/*vangl2*:mCherry+

(G+R+, yellow), *myf5*:GFP+/*vangl2*:mCherry- (G+, green) cells. (I) Relative expression of *fgfr1a*, *fgfr3* and *cd133/prominin1a (prom1a)* in sorted *myf5*:GFP+/*vangl2*:mCherry- (G+), *myf5*:GFP+/*vangl2*:mCherry+ (G+R+), *myf5*:GFP-/*vangl2*:mCherry+ (R+), *myf5*:GFP-/*vangl2*:mCherry- (NEG) cells and compared with whole zebrafish embryos at 6 and 24 hours post fertilization (hpf). *prom1a* is not detected in zebrafish ERMS. Graph is representative of n=2 independent ERMS.

Figure S6. *Related to Figure 6. vangl2*:mCherry labels self-renewing TPCs in zebrafish ERMS. (A,B) Transgenic zebrafish with primary ERMS expressing *vangl2(-5kb)*:mCherry along with *rag2*:GFP + *rag2*:kRASG12D. (C) Whole animal and (D) histology of syngeneic zebrafish engrafted with fluorescently-labeled ERMS imaged at 30 days post transplantation ($1x10^5$ unsorted tumor cells/animal). (E) FACS of *rag2*:GFP/*vangl2*:mCherry ERMS cells isolated from the transplant fish shown in C. (F) Sort purity of cells following FACS. (G-K) Sorted cell fractions were introduced into recipient fish at limiting dilution. Whole animal (G), histology (H) and FACS analysis (I) of fish engrafted with *rag2*:GFP+/*vangl2*:mCherry+ sorted cells. Sort purity of engrafted cells shown in lower left panel G. (J) Quantification of engraftment into syngeneic recipient animals (combined results from analysis of three independent ERMS, n=118 recipient fish total). *rag2*:GFP+/*vangl2*:mCherry+ (G+R+, yellow), *rag2*:GFP+/*vangl2*:mCherry- (G+, green) and *rag2*:GFP-/*vangl2*:mCherry+ (R+, red) tumor cells. (K) Graphical analysis of Extreme Limiting Dilution Analysis (ELDA) denoting overall engraftment rates at various cell dilutions. Dotted lines represent 95% confidence intervals. Estimated tumor propagating cell number for each cell fraction is indicated. ***$p<0.001$. (L) Sort purity of fluorescent-labeled ERMS cells isolated from tertiary recipient fish following two rounds of FACS. (M) Fluorescent image of fish engrafted with *rag2*:GFP+/*vangl2*:mCherry+ ERMS cells, establishing long-term and serial repopulating ability of Vangl2+ TPCs. Sort

purity of engrafted cells is indicated in lower left panel M (viability >96%). (N) Histology of fish shown in M. (O) Quantification of tumor engraftment by 90 days post transplantation with sorted ERMS cells, *rag2*:GFP+/*vangl2*:mCherry+ (G+R+, yellow) and *rag2*:GFP+/*vangl2*:mCherry- (G+, green) cells.

Figure S7. *Related to Figure 7.* RHOA acts downstream of VANGL2 to elicit rhabdosphere formation in Rh30 ARMS, RD and Rh36 ERMS cells. (A) Western blot analysis for VANGL2, RHOA and RAC1 protein in Rh30 cells grown as adherent (2D) cells or in sphere culture for 5 and 10 days. Relative protein expression was normalized to GAPDH. (B-G) Rh30 rhabdospheres stably infected with (B) scramble shRNA (shSCRM), (C) VANGL2 shRNA (shVL2(1)) (D) shSCRM + $RHOA^{V14}$, (E) shVL2 + $RHOA^{V14}$, (F) shSCRM + $RHOA^{N19}$, and (F) shVL2(1) + $RHOA^{N19}$. (H) Western blot analysis for epistasis performed in Rh30 cells stably infected with scramble shRNA (shSCRM) or VANGL2 shRNA (shVL2(1), shVL2(2)) +/- $RHOA^{V14}$ or $RHOA^{N19}$ expression vectors. Relative RHOA/RHOA-GTP protein is indicated for control and VANGL2 knock-down cells. GAPDH is used as a loading control and was used to normalize protein expression. (I) Quantification of Rh30 rhabdosphere colony growth at 10 days (10^4 cells plated per well). *p<0.05, **p<0.01, ***p<0.001, Student's t-test. Error bars represent standard deviation. (J) Western blot of total RAC1 and activated RAC1 (RAC1-GTP) in epistasis experiments performed in Rh30 cells stably infected with scramble shRNA (shSCRM) or VANGL2 shRNA (shVL2(1), shVL2(2)) +/- $RAC1^{V12}$ or $RAC1^{N17}$ expression vectors. GAPDH is used as a loading control. (K) Quantification of Rh30 rhabdosphere colony formation at 10 days (10^4 cells/plated per well). (L,O) Western blot analysis of RAC1 in 2D and 3D-rhabdosphere culture of RD (L) and Rh36 (D) ERMS cells. (M,O) Western blot of total RAC1 and activated RAC1 (RAC1-GTP) in RD (M) and Rh36 (P) ERMS cells stably infected with scramble shRNA (shSCRM) or VANGL2 shRNA (shVL2(1), shVL2(2)) +/- $RAC1^{V12}$ or

$RAC1^{N17}$. GAPDH is used as a loading control. (N,O) Quantification of rhabdosphere colony formation for RD cells (N) and Rh36 (Q) ERMS cells (10^4 cells/plated per well). Error bars represent standard deviation. All rhabdosphere colony formation assays are representative experiments showing average colony number over three technical replicates. Three independent experiments (n=3) were performed with the same effect observed across each biological replicates for each cell line.

Supplemental Table Legends

Table S1. ***Related to Figure 5.*** **Extreme limiting dilution analysis (ELDA) comparing** ***rag2*****:kRASG12D and** ***rag2*****:kRASG12D +** ***rag2*****:Vangl2 zebrafish ERMS.**

Table S2. ***Related to Figure 6/S6.*** **Extreme limiting dilution analysis (ELDA) comparing engraftment of ERMS cell subpopulations isolated from rag2:GFP/vangl2:mCherry transgenic tumors.** *rag2*:GFP+/*vangl2*:mCherry+ (G+R+), *rag2*:GFP+/*vangl2*:mCherry- (G+) and *rag2*:GFP-/*vangl2*:mCherry+ (R+) engraftment potential. Engraftment into tertiary (ERMS 3°) and quaternary (ERMS 4°) transplant fish.

Table S3. ***Related to Figure 6.*** **Extreme limiting dilution analysis (ELDA) comparing engraftment of ERMS cell subpopulations isolated from** ***myf5*****:GFP/*****vangl2*****:mCherry transgenic tumors.** *myf5*:GFP+/*vangl2*:mCherry+ (G+R+); *myf5*:GFP+/*vangl2*:mCherry- (G+) and *myf5*:GFP-/*vangl2*:mCherry+ (R+) engraftment potential.

Table S4. Human primers. ***Related to STAR Methods.***

Table S5. Zebrafish primers. ***Related to STAR Methods.***

Figure S1. ***Related to Figure 1.***

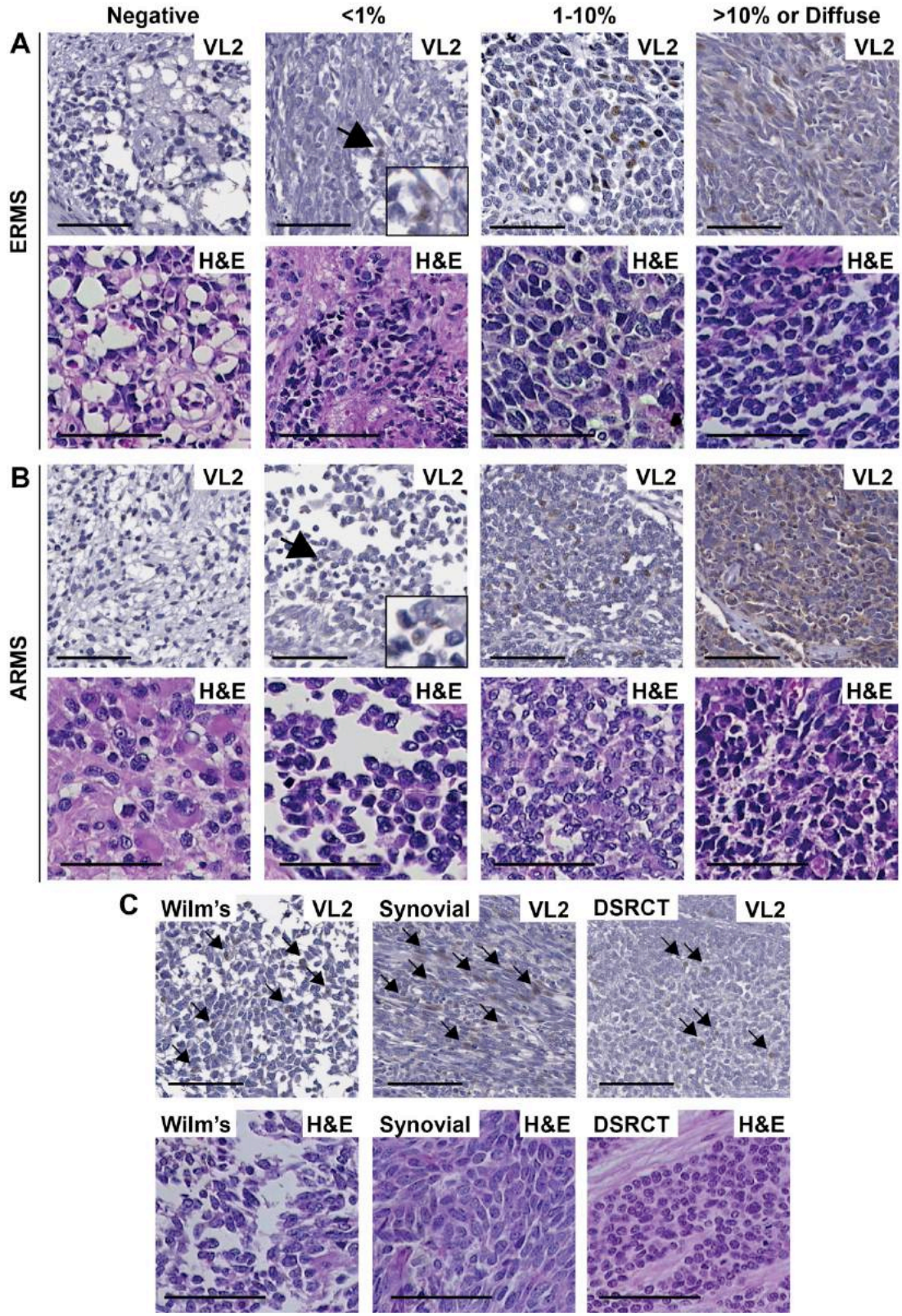

Figure S2. ***Related to Figure 3.***

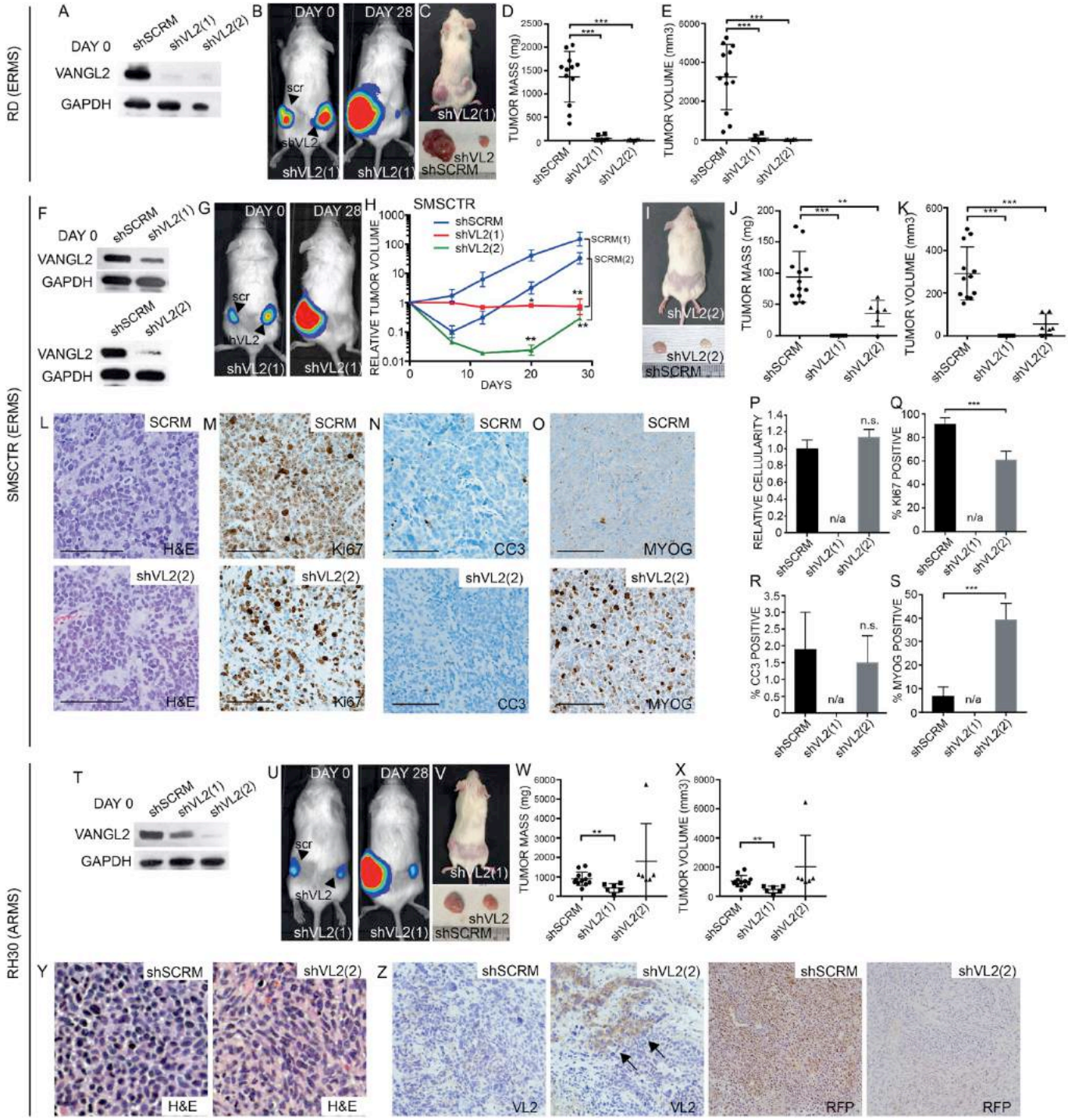

Figure S3. ***Related to Figure 4.***

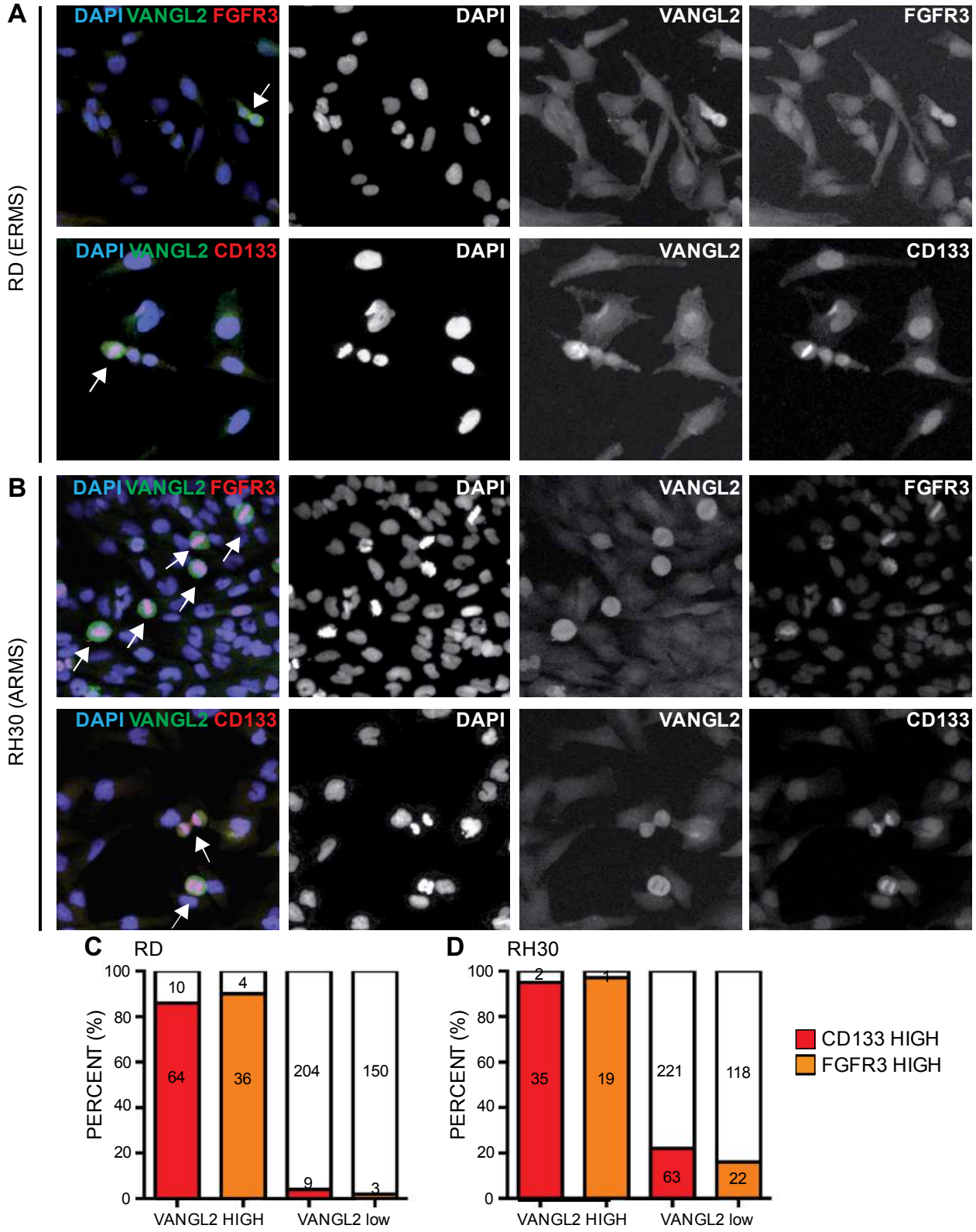

Figure S4. ***Related to Figure 5.***

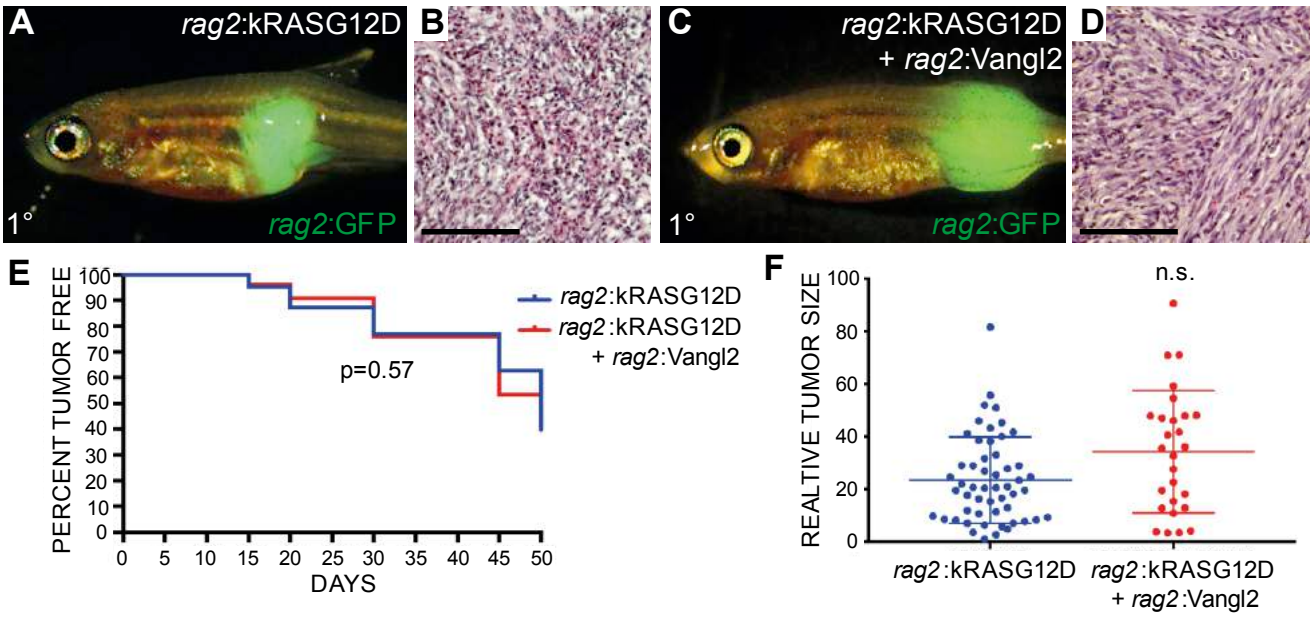

Figure S5. ***Related to Figure 6.***

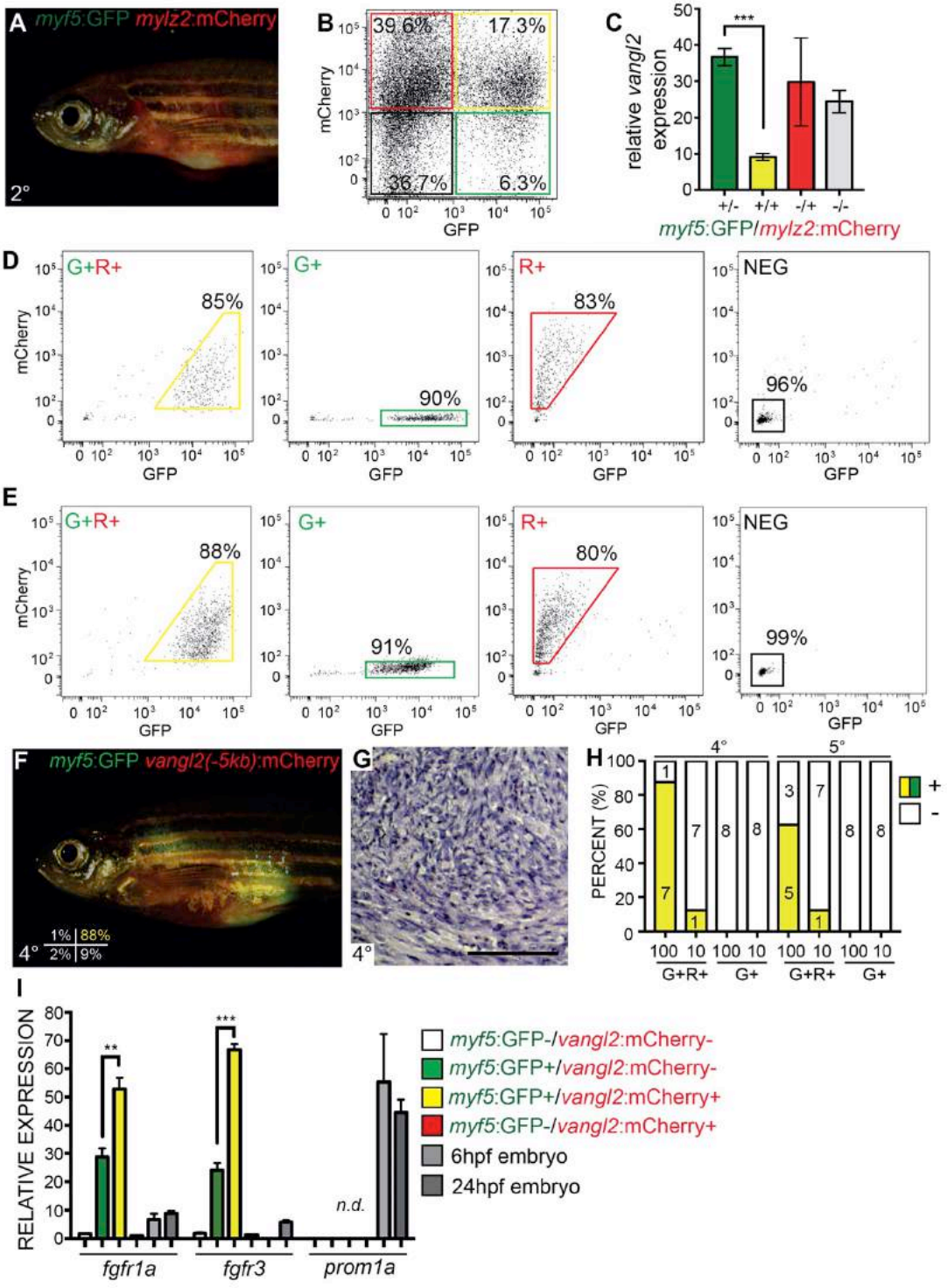

Figure S6. ***Related to Figure 6.***

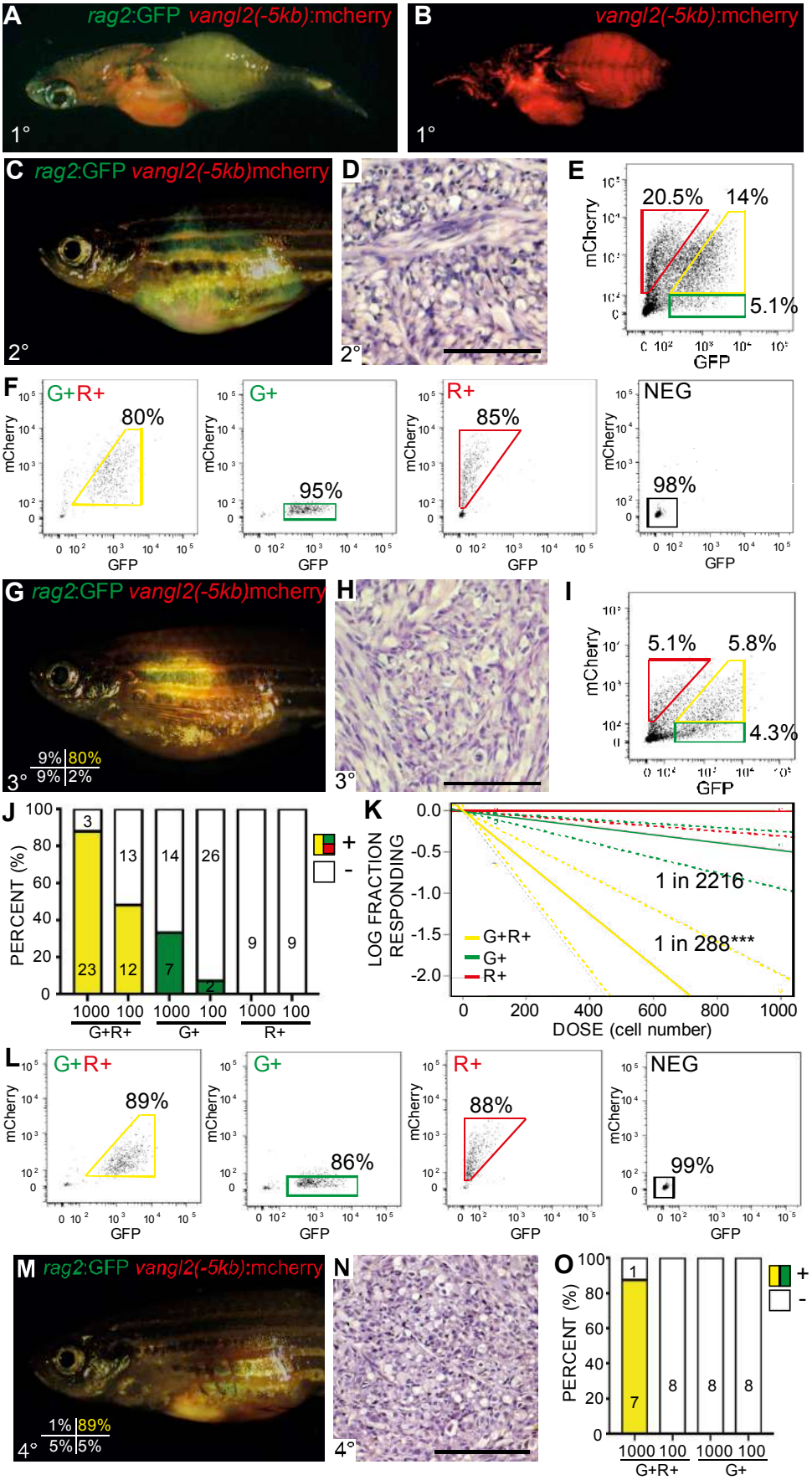

Figure S7. ***Related to Figure 7.***

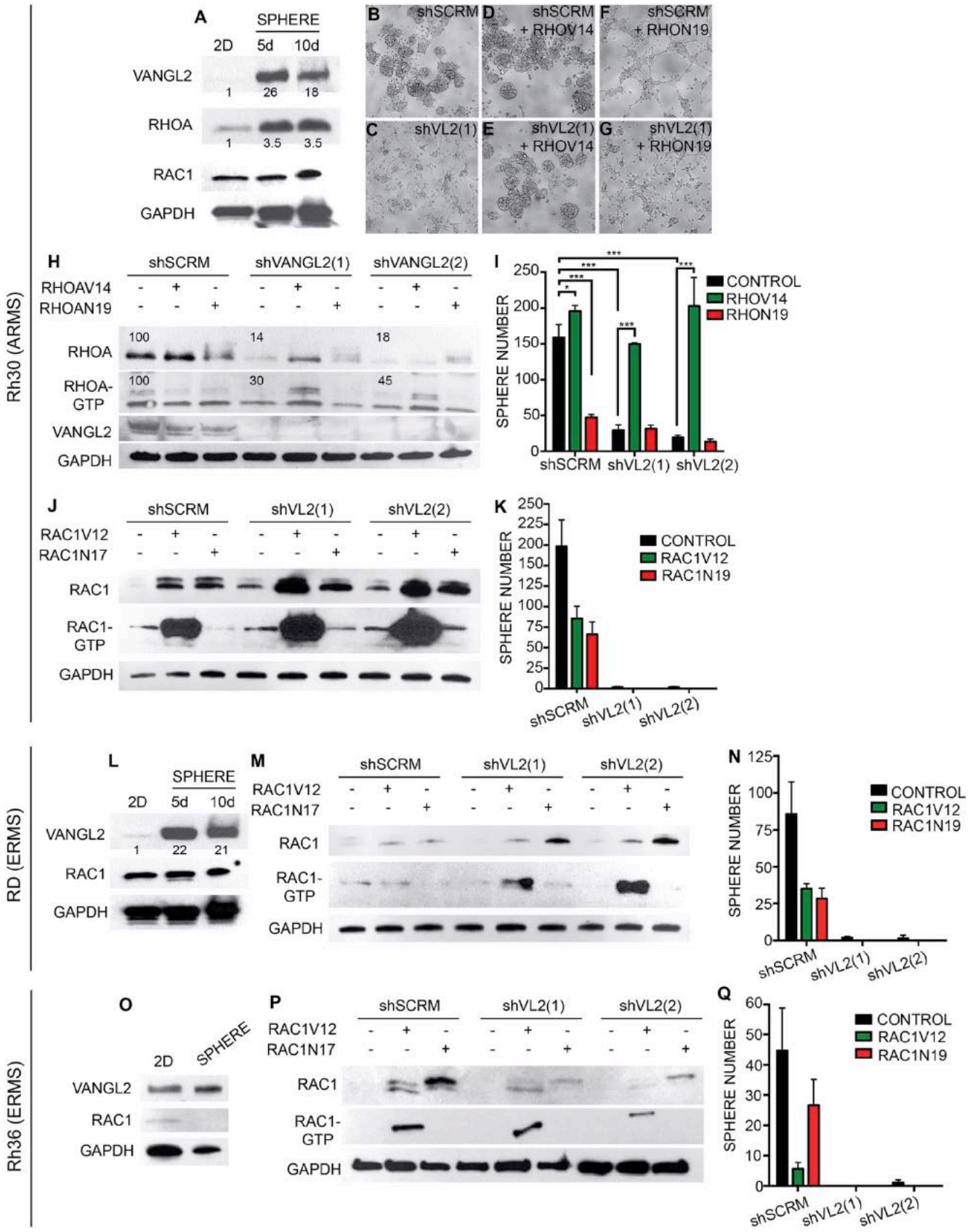

Table S1. ***Related to Figure 5.*** **Extreme limiting dilution analysis (ELDA) comparing *rag2*:kRASG12D and *rag2*:kRASG12D + *rag2*:Vangl2 zebrafish ERMS.**

rag2:kRASG12D

Cell #	Tumor 1	Tumor 2	Tumor 3
10000	6 of 6	6 of 6	6 of 8
1000	2 of 7	6 of 8	1 of 8
100	0 of 8	1 of 8	0 of 8
TPC #	2657	726	7388
95% CI	1053-6704	329-1600	3368-16209

TPC # **1 in 3590**

rag2:kRASG12D + *rag2*:Vangl2

Cell #	Tumor 1	Tumor 2	Tumor 3
10000	4 of 4	4 of 4	5 of 5
1000	7 of 7	8 of 8	6 of 9
100	4 of 9	3 of 10	2 of 10
TPC #	166	239	785
95% CI	66-415	104-549	371-1657

TPC # **1 in 396*****

Table S2. ***Related to Figure 6/S6.*** **Extreme limiting dilution analysis (ELDA) comparing engraftment of ERMS cell subpopulations isolated from rag2:GFP/vangl2:mCherry transgenic tumors.**

ERMS #1 3°

Cell #	**G+R+**	**G+**	**R+**
1000	7 of 7	0 of 6	0 of 5
100	4 of 7	0 of 10	0 of 5
TPC #	**1 in 241*****	N/A	N/A
95% CI	94-622	N/A	N/A

ERMS #1 4°

G+R+	**G+**
7 of 8	0 of 8
0 of 8	0 of 8
1 in 631***	N/A
290-1372	N/A

ERMS #2 3°

Cell #	**G+R+**	**G+**	**R+**
1000	10 of 10	6 of 9	0 of 4
100	6 of 10	2 of 10	0 of 4
TPC #	**1 in 109*****	1 in 785	N/A
95% CI	48-248	372-1658	N/A

ERMS #3 3°

Cell #	**G+R+**	**G+**	**R+**
1000	6 of 9	1 of 6	N/A
100	2 of 8	0 of 8	N/A
TPC #	**1 in 757***	1 in 6387	N/A
95% CI	356-1614	892-44338	N/A

Table S3. ***Related to Figure 6.*** **Extreme limiting dilution analysis (ELDA) comparing engraftment of ERMS cell subpopulations isolated from *myf5*:GFP/*vangl2*:mCherry transgenic tumors.**

ERMS #1 3°

Cell #	G+R+	G+	R+
100	6 of 9	0 of 9	0 of 5
10	3 of 7	0 of 10	0 of 5
TPC #	**1 in 65*****	N/A	N/A
95% CI	31-137	N/A	N/A

ERMS #1 4°

G+R+	G+
7 of 8	0 of 8
1 of 8	0 of 8
1 in 53***	N/A
25-114	N/A

ERMS #1 5°

G+R+	G+
5 of 8	0 of 8
1 of 8	0 of 8
1 in 98***	N/A
43-225	N/A

ERMS #2 3°

Cell #	G+R+	G+	R+
100	8 of 8	1 of 8	0 of 5
10	1 of 8	1 of 10	0 of 5
TPC #	**1 in 34*****	1 in 422	N/A
95% CI	15-75	103-1737	N/A

ERMS #3 3°

Cell #	G+R+	G+	R+
100	2 of 7	0 of 10	0 of 4
10	0 of 7	0 of 10	0 of 4
TPC #	**1 in 333***	N/A	N/A
95% CI	84-1325	N/A	N/A

ERMS #4 3°

Cell #	G+R+	G+	R+
100	8 of 8	4 of 8	0 of 6
10	5 of 10	1 of 10	N/A
TPC #	**1 in 15*****	1 in 135	N/A
95% CI	30-126	55-331	N/A

Table S4. Human primers. ***Related to STAR Methods.***

	PRIMER (5'-3')
GAPDH forward	GAGTCAACGGATTTGGTCGT
GAPDH reverse	GACAAGCTTCCCGTTCTCAG
MYOD forward	CGCGACGTAGACCTGACGGC
MYOD reverse	GTGGTCTTGCGCTTGCACGC
PAX7 forward	TGTGACCGAAGCACTGTGCCC
PAX7 reverse	AGCCGGTTCCCTTTGTCGCC
MYOG forward	CCTGCCGTGGGCGTGTAAGG
MYOG reverse	GGACTGCAGGAGGCGCTGTG
MCAD forward	CTTGCACTGTGCGGATCTCTC
MCAD reverse	TCCCAGGCACCTATGTGAC
MET forward	TTACGGACCCAATCATGAGC
MET reverse	ACTTCGCTGAATTGACCCAT
PAX3 forward	AGTGAGATTACGCGCTAG
PAX3 reverse	CCAGCGGAAGACCAGAAAC
VANGL2 forward	AGCGGCGGGAGCGTC
VANGL2 reverse	GAGGCACCTTCAGGAAGTCA

Table S5. Zebrafish primers. ***Related to STAR Methods.***

	PRIMER (5'-3')
vangl2 forward	AATCTGTGACCATCCAGGCTC
vangl2 reverse	TCACCACAGTCGTGGTTTCA
myf5 forward	CCAGACAGTCCAAACAACAGACC
myf5 reverse	TGAGCAAGCAGTGTGAGTAAGCG
myod forward	CAGTGGAGACTCTGATGCTTCCAG
myod reverse	AGCTGTCATAGCTGTTCCGTCTTC
pax7a forward	ACACCCGACGTTGAAAAGAG
pax7a reverse	TCACACACTCCGTCCTTCAG
myog forward	GTGGACAGCATAACGGGAACAG
myog reverse	TCTGAAGGTAACGGTGAGTCGG
mylz2 forward	ACCGCAGAGGAGATGAAGAA
mylz2 reverse	TCCGTGTGTGATGACGTAGC
c-met forward	GTCATCCAGGTGGTGGTTTC
c-met reverse	CGTTGTGATGCTGTGGAGAC
tnni2a forward	TCAGGCTCTGCTGGGCTCCA
tnni2a reverse	TACGCCAGTCGCCGACCTGT
acta1b forward	CTGAGCGCGGTTATTCTTTC
acta1b reverse	TCCAGAGCCACATAGCACAG
myh9a forward	GAGGGGTCCGAGCCAACTCC
myh9a reverse	AGAGCATGATGGCTGATAGCAGGT
arpc5b forward	TCATGGGTGCTCTACAGGCAGTATT
arpc5b reverse	AGCACCTTCAGCACCAGACCTTC
fgfr1a forward	TGGAAATCCTACACCGACGC
fgfr1a reverse	TGCTCTCGTACCTTGAAGCC
fgfr3 forward	GAAGATGAGGACGAGGCAGG
fgfr3 reverse	GTATTGGCAGCAGGAACAGC
prom1a forward	TGCTTTGGAAAACGGCACTG
prom1a reverse	AATCCAAAGTTCTCCGCGCT
18s forward	TCGCTAGTTGGCATCGTTTATG
18s reverse	CGGAGGTTCGAAGACGATCA